Automatica 165 (2024) 111651

Contents lists available at ScienceDirect

Automatica

journal homepage: www.elsevier.com/locate/automatica

Cooperative energy and time-optimal lane change maneuvers with minimal highway traffic disruption☆

Andres S. Chavez Armijos [a,*], Anni Li [a], Christos G. Cassandras [a], Yasir K. Al-Nadawi [b,1], Hidekazu Araki [b,1], Behdad Chalaki [b], Ehsan Moradi-Pari [b], Hossein Nourkhiz Mahjoub [b], Vaishnav Tadiparthi [b]

[a] Division of Systems Engineering, Boston University, Brookline, MA 02446, USA
[b] Honda Research Institute-US (HRI-US), Ann Arbor, MI 48103, USA

ARTICLE INFO

Article history:
Received 14 April 2023
Received in revised form 12 October 2023
Accepted 28 January 2024
Available online 12 April 2024

Keywords:
Connected autonomous vehicles
Decentralized cooperative control
Optimal control

ABSTRACT

We derive optimal control policies for a Connected Automated Vehicle (CAV) and cooperating neighboring CAVs to carry out a lane change maneuver consisting of a longitudinal phase where the CAV properly positions itself relative to the cooperating neighbors and a lateral phase where it safely changes lanes. In contrast to prior work on this problem, where the CAV "selfishly" only seeks to minimize its maneuver time, we seek to ensure that the fast-lane traffic flow is minimally disrupted (through a properly defined metric). Additionally, when performing lane-changing maneuvers, we optimally select the cooperating vehicles from a set of feasible neighboring vehicles and experimentally show that the highway throughput is improved compared to the baseline case of human-driven vehicles changing lanes with no cooperation. When feasible solutions do not exist for a given maximal allowable disruption, we include a time relaxation method trading off a longer maneuver time with reduced disruption. Our analysis is also extended to multiple sequential maneuvers. Simulation results show the effectiveness of our controllers in terms of safety guarantees and up to 16% and 90% average throughput and maneuver time improvement respectively when compared to maneuvers with no vehicle cooperation.

1. Introduction

Advancements in transportation technologies, including Connected Automated Vehicles (CAVs), have the potential to greatly enhance transportation networks by improving safety and comfort, reducing congestion, and increasing energy efficiency. In the realm of highway driving, autonomous car-following systems have seen significant developments in recent years, as outlined in Wang et al. (2016, 2015), Zhao et al. (2018). However, automating lane change maneuvers remains a challenging problem that has garnered increased attention (Bax et al., 2014; He et al., 2021; Nilsson et al., 2015). Existing work primarily focuses on controlling a single vehicle during the maneuver, lacking an analysis of the overall disruption effects on traffic flow.

The rise of CAVs presents an opportunity for cooperative maneuvers on multi-lane roads (Li et al., 2020; Luo et al., 2016; Mahjoub et al., 2017). Coordinated lane changes become especially crucial in heavy traffic conditions, where the cooperation of multiple vehicles can enable a broader range of feasible maneuvers, enhance safety, and improve throughput.

Solving cooperative multi-agent lane-changing maneuvers can take a centralized or decentralized approach. In the centralized method, a Control Zone (CZ) issues commands to all vehicles within a specified area. However, this can be computationally challenging. In contrast, the decentralized approach involves each agent computing its solution, which may result in conservative solutions and unwanted disruptions (Li et al., 2018).

Prior work, such as Chen et al. (2022), has provided time and energy-optimal solutions for lane-changing maneuvers. However, these approaches tend to be vehicle-centric, focusing on the maneuvering vehicle's optimization while neglecting the impact on

☆ Supported by the Honda Research Institute USA (HRI-USA), by The National Science Foundation (NSF), USA under grants ECCS-1931600, DMS-1664644, CNS-1645681, CNS-2149511, by AFOSR, USA under grant FA9550-19-1-0158, by ARPA-E, USA under grant DE-AR0001282, and by the MathWorks. The material in this paper was partially presented at the 25th IEEE Intelligent Transportation Systems Conference (ITSC), September 18th–October 12th, 2022, Macau, China. This paper was recommended for publication in revised form by Associate Editor Antonella Ferrara under the direction of Editor Thomas Parisini.

* Corresponding author.
E-mail addresses: aschavez@bu.edu (A.S. Chavez Armijos), anlianni@bu.edu (A. Li), cgc@bu.edu (C.G. Cassandras), behdad_chalaki@honda-ri.com (B. Chalaki), emoradipari@honda-ri.com (E. Moradi-Pari), hnourkhizmahjoub@honda-ri.com (H.N. Mahjoub), vaishnav_tadiparthi@honda-ri.com (V. Tadiparthi).

[1] Y. K. Al-Nadawi and H. Araki were with HRI during the period of this work.

https://doi.org/10.1016/j.automatica.2024.111651
0005-1098/

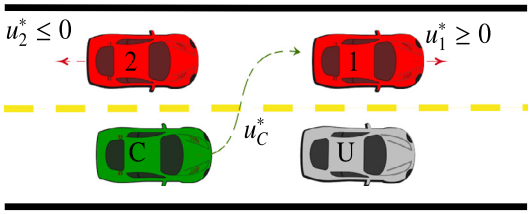

Fig. 1. The basic lane-changing maneuver process.

other vehicles. This approach can lead to traffic flow slowdowns in congested scenarios.

Our paper addresses these limitations by adopting a system-centric approach, balancing the needs of the individual vehicle with the overall traffic flow. We focus on multiple sequential lane-changing maneuvers, considering both vehicle position and speed disruption. Our analysis aims to improve traffic throughput and minimize disruptions in various traffic conditions.

In summary, this paper presents a comprehensive approach to cooperative lane-changing maneuvers, combining system-centric and vehicle-centric objectives. We consider both position and speed disruption and aim to enhance traffic flow in different scenarios.

In previous work, Chen et al. (2022) provided a time and energy optimal solution for the maneuver shown in Fig. 1, in which the controlled vehicle C attempts to overtake an uncontrollable vehicle U by using the left lane to pass. A decentralized solution is provided based on cooperation and communication with two neighboring vehicles (vehicles 1 and 2) to minimize the total maneuver time and subsequently determine trajectories that minimize the energy consumed by all three cooperating vehicles. This approach applies to a wider range of scenarios relative to those in Kamal et al. (2013), Luo et al. (2016), Nilsson et al. (2017).

However, by seeking to minimize C's maneuver time, Chen et al. (2022) adopt a *vehicle-centric* (selfish) viewpoint which ignores the effect of the maneuver on all remaining vehicles. As a result, since vehicle 2 typically decelerates to allow C to get ahead of it, this deceleration may cause a traffic flow slowdown in the left lane which can negatively impact throughput, especially in congested scenarios. Moreover, the analysis assumes that vehicles 1 and 2 are predetermined rather than being optimally selected among a set of possible cooperation candidates.

The main contribution of this paper is the alleviation of the aforementioned limitations in such *selfish* maneuvers by adopting an optimality viewpoint that combines *system-centric* objectives with vehicle-centric ones, as introduced in Chavez Armijos et al. (2022). This provides a decentralized optimal solution where our optimal controller design includes the social optimality goal of ensuring that the resulting traffic throughput on the highway is improved by adding vehicles to the fast lane while (i) limiting the "disruption" that cooperation among multiple vehicles on the road can cause on the fast lane traffic flow, and (ii) determining an optimal pair of cooperating vehicles, which play the role of 1 and 2 in Fig. 1, within a set of feasible such candidates. Additionally, we focus on the realization of *multiple* sequential lane-changing maneuvers under the assumption of cooperation with surrounding vehicles.

The disruption metric introduced in Chavez Armijos et al. (2022) considers how the *positions* of vehicles in the fast lane are disrupted relative to the "ideal" trajectories where fixed speeds are maintained. The associated disruption in their *speeds* is, however, not taken into account and this can be shown to allow for significant slowdowns in the traffic flow in certain situations. A key contribution of this paper is to alleviate this limitation in Chavez Armijos et al. (2022) by employing a disruption metric that includes both vehicle position and speed. This necessitates a new analysis for the problem of deriving time and energy-optimal maneuvers while also ensuring throughput improvements under different traffic densities. This paper provides this analysis, considers the sensitivity of the resulting algorithm to the aforementioned traffic densities, and makes use of a new estimate of the fast lane desired speed based on the speeds from the cooperative vehicle sets.

As in Chen et al. (2022), we decompose the maneuver into a longitudinal component followed by a lateral component. In the longitudinal part, our approach is based on first determining an optimal maneuver time for C subject to all safety and speed and acceleration constraints for C, 1, and 2 (see Fig. 1) and such that C attains a desired final speed that matches that of the fast lane traffic flow. We then solve a fixed terminal time decentralized optimal control problem for each of the two cooperating vehicles in which energy consumption is minimized while penalizing the deviation of 1 and 2 from the fast lane desired speed. In the lateral phase, we solve a decentralized optimal control problem seeking to jointly minimize the time and energy consumed which is no different than the one presented in Chen et al. (2022). Our analysis also allows the determination of a vehicle pair that results in minimal acceleration/deceleration for them. This minimizes the possibility of excessive braking or deceleration of the rear vehicle in the pair (2 in Fig. 1), quantified through an appropriate "disruption metric". An interesting consequence of our analysis is that it leads to vehicles forming natural platoons that dictate the free-flow speed of the fast lane on a two-lane highway.

The rest of the paper is organized as follows. Section 2 presents the formulation of the longitudinal lane-change maneuver problem. In Section 3, a complete optimal control solution to coordinate the longitudinal portion of the lane change maneuver is obtained. Section 4 describes the lateral portion of a lane-changing maneuver. Section 5 provides simulation results for several representative examples and we conclude with Section 6.

2. Problem formulation

In this section, we present a system-centric problem formulation of the cooperative maneuver setting in Fig. 1. We decompose the maneuver into a longitudinal and a lateral component. The former includes the determination of a minimally disrupting cooperative pair (playing the role of 1 and 2 in Fig. 1) while minimizing the deviation from the fast lane desired speed.

Let C be the vehicle that initiates an automated maneuver. This can be manually triggered by the driver of C deciding to overtake vehicle U or automatically triggered by a given distance detected from an uncontrollable vehicle U ahead of C, as shown in Fig. 2. Assuming that all vehicles other than U are CAVs, we will henceforth refer to them as such.

2.1. Cooperative vehicle set

Let $S(t)$ be the set of potential cooperating vehicles in the fast lane for CAV C during its lane change maneuver. This set is defined by the parameters L_r (distance in the rear of C) and L_f (distance in front of U) which are typically selected to include all vehicles within a given communication range.

Using the longitudinal position $x_i(t)$ of vehicle i relative to a reference origin O, we define $S(t)$ as:

$$S(t) := \{i \mid x_C(t) - L_r \leq x_i(t) \leq x_U(t) + L_f\} \quad (1)$$

where $x_i(t)$ is the longitudinal position of CAV i. We order the N CAVs in $S(t)$ by index from furthest ahead of C to nearest, so $i+1$

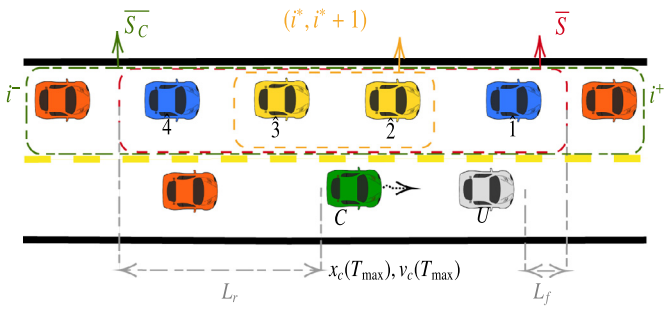

Fig. 2. Cooperative vehicle sets $\bar{S}_C$, $\bar{S}$, and optimal CAV subset $(i^*, i^*+1) \in \bar{S}_C$ selection diagram.

follows i. To simplify, once we determine N members of $S(t)$, we order their indices in ascending order, making $S(t) = 1, \ldots, N$. This setup helps us recognize cooperating pairs as $(i, i+1)$, allowing CAV C to merge between them. However, this excludes the possibility of CAV C changing lanes ahead of the first vehicle in $S(t)$ or behind the last. To address this, we extend the set as follows: We introduce $S^+(t) = \{i \mid x_i(t) > x_U(t) + L_f\}$ and designate i^+ to be the CAV immediately ahead of 1 in $S(t)$ if $S^+(t) \neq \emptyset$. Otherwise, i^+ is a "virtual" CAV with $x_{i^+}(t) = \infty$. Similarly, $S^-(t) = \{i \mid x_i(t) < x_C(t) - L_r\}$, and i^- is the CAV immediately behind the last vehicle in $S(t)$ if $S^-(t) \neq \emptyset$; otherwise, i^- is a "virtual" CAV with $x_{i^+}(t) = -\infty$. This leads to the extended set:

$$S_C(t) = S(t) \cup \{i^+, i^-\} \tag{2}$$

We rewrite $S_C(t)$ as $\{0, 1, \ldots, N, N+1\}$, assigning 0 to i^+ and $N+1$ to i^-. We will select an optimal pair, as described later, to be a subset $\{i^*, i^*+1\}$ of this set, with $i^* \in \{0, 1, \ldots, N\}$.

Construction of Cooperative Set. To determine $S_C(t)$ without unnecessary computation, we overestimate it by assuming constant speeds in $[t_0, T_{\max}]$, where $T_{\max}$ is a maximum tolerable maneuver time. Thus, we obtain $\bar{S}(T_{\max})$ by evaluating it on (1) with $x_i(T_{\max}) = x_i(t_0) + v_i(t_0)T_{\max}$. By adjusting L_f, L_r, and $T_{\max}$, we can include any desired number of candidate vehicles in $\bar{S}$, subject to C's communication range. Finally, the equivalent over-approximated set is defined as

$$\bar{S}_C = \bar{S}(T_{\max}) \cup \{i^+, i^-\} \tag{3}$$

If multiple maneuvers are to be executed, we index them by $k = 1, 2, \ldots$ and write $S_C^k(t)$ to represent the associated set corresponding to CAV C, which initiates the maneuver. We first limit ourselves to the simpler notation $S_C(t)$.

2.2. Fast lane desired speed

We define fast lane desired speed as the average speed at which the traffic travels on a lane or a road segment. To design a policy to perform minimally disrupting lane changes, it is necessary to estimate the fast lane desired speed from the perspective of the ego vehicle C. However, due to limitations of observability and sensing range, we can define the fast lane desired speed v_{flow} of the fast lane at time t as a convex combination (with weighting factor ω) of the average speed of the vehicles in the set $S_C(t)$ and the maximum allowable speed of the road. Thus, letting $\|S_C(t)\|$ be the cardinality of $S_C(t)$, set

$$v_{S_C}(t) = \frac{1}{\|S_C(t)\|} \sum_{i \in S_C(t)} v_i(t) \tag{4}$$

and define

$$v_{flow}(t) = \omega v_{S_C}(t) + (1-\omega) v_{\max} \tag{5}$$

Practically, we can think of ω as an "aggressiveness factor" that controls the target speed that each of the vehicles involved in a cooperative maneuver would try to reach. Specifically, when $v_{\text{flow}}(t)$ is closer to $v_{\max}$, the cooperative vehicles will try to accelerate more aggressively to reach higher speeds, while when $v_{\text{flow}}(t)$ is closer to $v_{S_C}(t)$, the vehicles will try to match the average speed of nearby vehicles more closely. This allows the tuning of the aggressiveness of the cooperative maneuver while still taking into account the actual traffic conditions.

2.3. Vehicle dynamics

For every vehicle $i \in S(t)$ its dynamics take the form

$$\dot{x}_i(t) = v_i(t), \quad \dot{v}_i(t) = u_i(t) \tag{6}$$

where, in addition to $x_i(t)$, we define $v_i(t)$ and $u_i(t)$ to be vehicle i's velocity and (controllable) acceleration respectively. Without loss of generality, we define the origin for CAV i involved in a maneuver to be the position $x_C(t_0)$ of CAV C, where t_0 denotes the time at which the maneuver is triggered. We will use t_f to denote the time when the longitudinal maneuver is complete. The control and speed are constrained as follows:

$$u_{i_{\min}} \leq u_i(t) \leq u_{i_{\max}}, \quad \forall t \in [t_0, t_f] \tag{7a}$$

$$v_{i_{\min}} \leq v_i(t) \leq v_{i_{\max}}, \quad \forall t \in [t_0, t_f] \tag{7b}$$

where $v_{i_{\max}} > 0$ and $v_{i_{\min}} > 0$ denote the maximum and minimum speed allowed, usually determined by the rules of the highway. Similarly, $u_{i_{\max}} > 0$ and $u_{i_{\min}} < 0$ are i's maximum and minimum acceleration control for vehicle i.

2.4. Safety constraints

Let $\delta_i(v_i(t))$ be the speed-dependent safety distance of CAV i, defined as the minimum required distance between i and its immediately preceding vehicle:

$$\delta_i(v_i(t)) = \varphi v_i(t) + \varepsilon, \tag{8}$$

where φ is a constant value that denotes the reaction time (usually defined as $\varphi = 1.8\,\text{s}$ Vogel (2003)), ε is a constant, and $\delta_i(v_i(t))$ is specified from the center of i to the center of its preceding vehicle. We can now define all safety constraints that must be satisfied during a lane-changing maneuver of C when cooperating with any two CAVs $(i, i+1)$:

$$x_U(t) - x_C(t) \geq \delta_C(v_C(t)), \quad \forall t \in [t_0, t_f] \tag{9a}$$

$$x_i(t) - x_{i+1}(t) \geq \delta_{i+1}(v_{i+1}(t)), \quad \forall t \in [t_0, t_f] \tag{9b}$$

$$x_C(t_f) - x_{i+1}(t_f) \geq \delta_{i+1}(v_{i+1}(t_f)), \tag{9c}$$

$$x_i(t_f) - x_C(t_f) \geq \delta_C(v_C(t_f)) \tag{9d}$$

2.5. Traffic disruption

We aim to quantify the extent to which a successful lane-changing maneuver can disrupt fast-lane traffic. To achieve this, we introduce the concept of *disruption*:

Definition 1 (*Single Vehicle Disruption*)**.** For any $t_f > t_0$, let $x_i(t_f)$ be the terminal position of vehicle i, determined by some control policy $u_i(t)$, $t \in [t_0, t_f]$. For any vehicle $i \in S_C(t)$, the disruption metric $D_i(t)$ at time $t > t_0$ is defined as the convex combination:

$$D_i(t) = \gamma_x d_x^i(t) + \gamma_v d_v^i(t) \tag{10}$$

where $d_x^i(t)$ and $d_v^i(t)$ are the contributions of position and speed disruption, respectively, and $\gamma_x, \gamma_v \in [0, 1]$, $\gamma_x + \gamma_v = 1$.

The constants γ_x and γ_v are the weighted contributions of one component over the other, making them tunable parameters to control which aspect of disruption is more critical to minimize. This definition provides a quantifiable metric for the disruption caused by a vehicle i during a highway maneuver. The position component $d_x^i(t)$ measures the deviation from an ideal undisrupted trajectory, while the speed component $d_v^i(t)$ measures the deviation from the desired lane speed.

To accurately define the dimensionality of the convex combination for a lane-changing maneuver, we derive each disruption contribution along with its corresponding normalization factor below.

Position Disruption. The position disruption $d_x^i(t)$ is defined as the square of the disruption caused to i due to an acceleration/deceleration control $u_i(t)$ relative to its undisrupted final position. We express it as:

$$d_x^i(t) = (x_i(t) - [x_i(t_0) + v_i(t_0)(t - t_0)])^2 \tag{11}$$

This equation quantifies the difference between the actual position $x_i(t)$ of vehicle i under a given control policy at time t and its ideal position, achieved by maintaining a constant speed $v_i(t_0)$. This ideal scenario minimizes energy consumption due to any acceleration/deceleration.

To normalize $d_x^i(t)$ in (11), we define:

$$\gamma_x = \frac{\gamma}{(d_{x_{\max}}(t))^2} \tag{12}$$

Here, $\gamma \in [0, 1]$ is a tuning parameter and $d_{x_{\max}}(t)$ is the maximum possible position disruption that vehicle i could generate over $[t_0, t_0 + t]$, i.e., under minimum speed and minimum acceleration (maximum deceleration). Thus, we define two cases: first, the maximum distance traveled under minimum acceleration, and second, the maximum distance traveled under minimum acceleration before the vehicle attains its minimal longitudinal speed. Therefore, $d_{x_{\max}}$ takes the form

$$d_{x_{\max}}(t) = \begin{cases} d_{u_{\min}}, & \text{if } u_{\min}(t - t_0) + v_i(t_0) \geq v_{min} \\ d_{v_{\min}}, & \text{otherwise.} \end{cases} \tag{13}$$

with

$$d_{u_{\min}} = v_i(t_0)(t - t_0) - \left(v_i(t_0)(t - t_0) + 0.5u_{\min}t^2\right)$$

$$d_{v_{\min}} = v_i(t_0)(t - t_0) - v_{\min}\left((t - t_0) - \frac{v_{min} - v_i(t_0)}{u_{\min}}\right) + \frac{v_{i\min}^2 - v_i(t_0)^2}{2u_{\min}}$$

Speed Disruption. We define the speed disruption contribution $d_v^i(t)$ as the deviation of vehicle i's speed $v_i(t)$ from the fast lane's desired speed v_{flow}. It is expressed as:

$$d_v^i(t) = \left(v_i(t) - v_{flow}\right)^2 \tag{14}$$

with its corresponding normalization factor defined as

$$\gamma_v = \frac{1 - \gamma}{\max\{(v_{\min} - v_{flow})^2, (v_{\max} - v_{flow})^2\}}.$$

where $\gamma \in [0, 1]$ is the same weight parameter in (12).

Now, let us define the triplet of vehicles involved in a lane-changing maneuver as $S_i = \{C, i, i + 1\}$. We can define the total disruption produced by S_i as follows:

Definition 2 (*Total Disruption*)**.** The total disruption $D_S(t)$ is defined as the convex combination of the single vehicle disruption contributions $D_i(t)$ defined in (10):

$$D_{S_i}(t) = \sum_{j \in S_i} \zeta_j D_j(t), \tag{15}$$

where, $\zeta_j \in [0, 1]$ are the weights such that $\sum_{j \in S_i} \zeta_j = 1$.

The weights in (15) allow for the consideration of different potential effects that each cooperating CAV will have on the overall total disruption. For example, if ζ_{i+1} is large relative to ζ_i and ζ_C, it places more weight on the disruption caused to the rear vehicle, which allows C to move ahead of it, potentially affecting other vehicles behind $i + 1$.

It is important to note that (15) is a quadratic disruption metric that depends on factors such as the total maneuver time length $t_f - t_0$, the terminal positions $x_i(t_f)$, and the terminal speeds $v_i(t_f)$ for every CAV i involved in the maneuver. This metric implicitly penalizes various disruptions, including the time it takes for vehicles to regain fast lane speed after a lane-changing maneuver and the potential chain reaction of slowdowns. If multiple maneuvers are considered (indexed by $k = 1, 2, \ldots$), we can minimize an aggregate metric D_{Total} by summing individual disruptions $D_S^k(t)$.

2.6. Optimal maneuver objectives

We consider two objectives for the longitudinal maneuver problem: first, we wish to minimize the maneuver time t_f experienced by CAV C and its cooperating vehicles; second, we wish to minimize the energy consumption of each of the three cooperating CAVs, i.e., C, i and $i+1$. At the same time, we must satisfy the safety constraints (8) and vehicle constraints (7). Finally, we must ensure that the disruption metric (15) does not exceed a given threshold D_{th}. Thus, among all candidate cooperating pairs $(i, i+1)$ for which these objectives are achieved we select the one that solves the disruption minimization problem:

$$S_i^* = \underset{S_i \in \tilde{S}_C}{\operatorname{argmin}} D_{S_i}(t_f^*) \tag{16a}$$

$$\text{s.t. } D_{S_i}(t_f^*) \leq D_{th} \tag{16b}$$

where $D_C^*(t)$ denotes the minimum disruption which corresponds to the triplet $S_i^* = \{C, i^*, i^* + 1\}$ with minimum disruption.

3. Longitudinal optimal control solution

In this section, we present a detailed solution approach with the following key elements: (i) We specify the objective functions J_C for CAV C and J_i for any $i \in S_C(t)$. (ii) We obtain the optimal cooperating pair (i^*, i^*+1) by evaluating the total disruption that each possible cooperative triplet might produce. (iii) We include a time relaxation on the optimal maneuver time t_f^* so that, if a feasible solution does not exist, we seek one for a relaxed value $t_f' > t_f^*$. The relaxation process captures the trade-off between the "selfish" goal of C to minimize its maneuver time and the system-wide "social" goal of minimizing traffic flow disruptions while ensuring an increase in throughput by adding vehicles to the fast lane. The overall description of the solution process for the optimal maneuver ensuring a minimal disruption that does not exceed a given threshold D_{th} is given in Fig. 3. However, we describe each step in detail in the subsequent subsections.

3.1. CAV C optimal trajectory

Given a CAV C traveling behind an uncontrolled vehicle U, a "start maneuver" request is sent to surrounding vehicles, and the starting time t_0 is defined when $x_U(t) - x_C(t) \leq d_{\text{start}}$, where d_{start} denotes the minimum distance at which CAV C decides to initiate a lane-changing maneuver. It is important to point out that at that instant the values of the optimal maneuver time and the entire optimal trajectory of C can be evaluated, which also enables planning the complete solution to the problem.

We now define the optimal control problem (OCP) for CAV C as follows:

$$\min_{t_f, \{u_C(t)\}} \frac{w_v}{2}(v_C(t_f) - v_{flow})^2 + \int_{t_0}^{t_f} \left(w_t + \frac{w_u}{2}u_C^2(t)\right) dt \tag{17a}$$

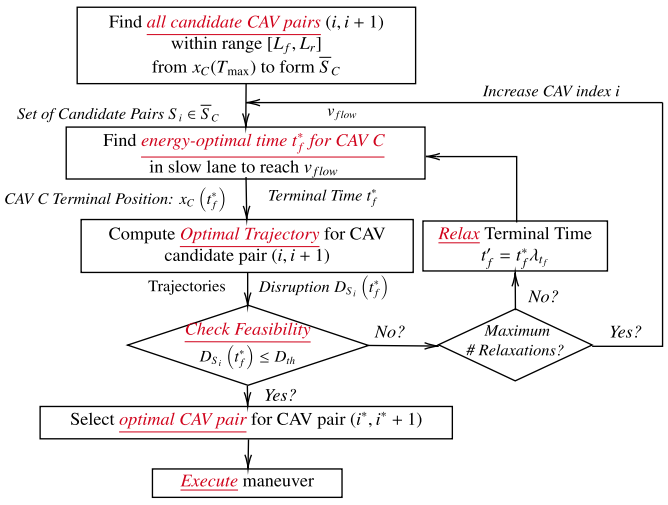

Fig. 3. Cooperative maneuver flow diagram.

s.t. (6), (7),

$$x_U(t) - x_C(t) \geq \delta_C(v_C(t)), \ \forall t \in [t_0, t_f], \tag{17b}$$

$$t_0 \leq t_f \leq T_{\max} \tag{17c}$$

Here, $w_{\{t,\ v,\ u\}}$ are adjustable non-negative weights with appropriate dimensions that place a relative emphasis on each of the three objective function components with respect to each other during the optimization process. Thus, we can penalize longer maneuver times, deviation from the desired speed, and energy consumption to trade off among these metrics as desired. The desired speed value of $v_C(t_f)$ is set to v_{flow} as defined in (5) using $v_{\bar{S}_C}$ with $\bar{S}_C$ defined in (3). Constraint (17b) capture the safe distance constraint (9a) between C and U (assuming that the position and speed of U can be sensed or estimated by C). Similarly, in constraint (17c), we specify $T_{\max}$ as the maximum tolerable time to perform a lane-changing maneuver. In practice, if constraint (17c) cannot be met for a given $T_{\max}$, CAV C has the option of either relaxing this value (as detailed in Section 3.4) or simply aborting the maneuver. Finally, note that problem (17) is solved given the initial position and speed of CAV C.

The solution of this OCP can be analytically obtained, as shown in the Appendix, through standard Hamiltonian analysis similar to OCPs formulated and solved in Chen et al. (2022).

It is worth pointing out that depending on the weights w_i and the starting distance d_{start} of the maneuver, the form of the corresponding optimal trajectory can be either strictly *accelerating* or first *decelerating* followed by an accelerating component so that (9a) is satisfied regardless of the initial conditions of CAV C. Intuitively if there is adequate distance ahead of C, it can accelerate at a maximal rate to attain $v_c(t_f) = v_{flow}$; otherwise, it needs to first decelerate to create such an adequate distance ahead of it and then accelerate to minimize the terminal speed cost in (17a).

3.2. Optimal trajectories for CAV candidates $(i, i+1)$

For any CAV i other than C, we define its objective function to be:

$$J_i(u_i(t)) = \beta(v_i(t_f^*) - v_{flow})^2 + \int_{t_0}^{t_f^*} \frac{1}{2} u_i^2(t) dt$$

where t_f^* was determined from (17) and

$$\beta = \frac{\alpha_v \max\left\{u_{i_{\min}}^2, u_{i_{\max}}^2\right\}}{(1-\alpha_v)}$$

with α_v being a constant weight factor with appropriate dimensions that penalizes speed deviation from the desired v_{flow} relative to an energy consumption metric so that CAV i (where $i = i^*$ or $i = i^*+1$ when the optimal cooperative pair has been found) solves the following two fixed terminal time OCPs for CAV i and $i+1$ respectively:

$$\min_{\{u_i(t)\}} \beta(v_i(t_f^*) - v_{flow})^2 + \int_{t_0}^{t_f^*} \frac{1}{2} u_i^2(t) dt \tag{18a}$$

s.t. (6), (7)

$$x_{i-1}(t) - x_i(t) \geq \delta_i(v_i(t)), \ \forall t \in [t_0, t_f^*], \tag{18b}$$

$$x_{i-1}(t) = x_{i-1}(t_0) + v_{i-1}(t)(t - t_0) \tag{18c}$$

$$x_i(t_f^*) - x_C(t_f^*) \geq \delta_C(v_C(t_f^*)) \tag{18d}$$

where $x_i(t_f^*)$ is the terminal position for vehicle i under the safety considerations of a potential vehicle ahead of i (labeled $i-1$) for all $t \in [t_0, t_f^*]$, as well as the safety constraint for the terminal position of CAV C computed by the OCP in (17).

$$\min_{\{u_{i+1}(t)\}} \beta(v_{i+1}(t_f^*) - v_{flow})^2 + \int_{t_0}^{t_f^*} \frac{1}{2} u_{i+1}^2(t) dt \tag{19a}$$

s.t. (6), (7)

$$x_C(t_f^*) - x_{i+1}(t_f^*) \geq \delta_{i+1}(v_{i+1}(t_f^*)) \tag{19b}$$

$$v_{i+1}(t_f^*) \geq v_{th} \tag{19c}$$

Here, the terminal position for $i+1$ is only constrained by CAV C in (19b). Additionally, in (19) we remove the safety constraint (9b) between i and $i+1$ due to Thm. 1 in Chen et al. (2022) where it is shown that in an optimal maneuver, CAV i does not accelerate and CAV $i+1$ does not decelerate.

Lastly, in (19c) we include a terminal constraint on the minimum allowable terminal speed for $i+1$ with the introduction of v_{th}, which differs from v_{flow} in that it prevents $i+1$ from reaching a terminal speed which is much lower than v_{flow}. Ignoring the v_{th} constraint can lead to a subtle pattern of inefficient maneuvers we observed when implementing our prior controllers in Chavez Armijos et al. (2022): when a CAV i^*+1 decelerates to a much lower speed than the fast lane desired speed to allow lane changes, it may repeatedly decelerate to allow multiple new maneuvering CAVs to get ahead of it with short maneuver times. This can be very effective in terms of the objective of minimizing maneuver times, at the expense of dramatic traffic disruptions and ultimate high congestion in the fast lane.

3.3. Selection of optimal cooperative pair (i^*, i^*+1)

The optimal cooperative pair (i^*, i^*+1) among all $i \in \bar{S}_C$ in (3) is the one that minimizes the disruption metric in (15) by selecting the terminal states $\left(x_i(t_f^*), v_i(t_f^*)\right)$ for every pair i and $i+1$ resulting in minimal disruption.

The solution of (18) and (19) for every pair $(i, i+1)$ respectively provides the optimal terminal positions $x_i(t_f^*)$, $x_{i+1}(t_f^*)$ and terminal speeds $v_i(t_f^*)$, $v_{i+1}(t_f^*)$ that provide the inputs for computing the disruption metric $D_{S_i}(t)$, defined in (15), for the triplet $S_i \in \bar{S}_C$.

Specifically, we solve (16) by discretizing the set of candidate vehicles $\bar{S}_C$. Thus, (16) is solved by comparing the values of $D_{S_i}(t_f^*)$ obtained over a finite set consisting of vehicle pairs $(i, i+1)$ that satisfy the disruption constraint.

Remark 1. If no solution to (16) is found, it is still possible to derive a solution based on the analysis in Chen et al. (2022), with no consideration of disruption. Alternatively, we may proceed with the time relaxation process described in Section 3.4.

3.4. Maneuver time relaxation

It is possible that no solution to (18), (19), or (16) may be found. The most common reason is that the optimal maneuver end time t_f^*, determined by CAV C at the first step of the solution approach, is too short to allow C to reach a speed sufficiently close to v_{flow} and for cooperating CAVs to adjust their positions to satisfy the safety constraints in (8). In such cases, it is possible to perform a relaxation of t_f^* obtained through (17) by trading it off against the energy consumption due to the maneuver extension. Thus, the new terminal time is given as $t_f' = t_f \lambda_{t_f}$ where $\lambda_{t_f} > 1$ is a relaxation factor. Observe that this time modification changes the form of the OCP (17) since the terminal time is now fixed at $t_f' > t_f^*$ and the solution will lead to a new terminal position $x_c(t_f')$ for CAV C. The new fixed terminal time OCP formulation is as follows:

$$\min_{\{u_C(t)\}} \beta(v_{i+1}(t_f') - v_{flow})^2 + \int_{t_0}^{t_f'} \frac{1}{2} u_C^2(t) dt \tag{20a}$$

s.t. (6), (7), and

$$x_U(t) - x_C(t) \geq \delta_C(v_C(t)), \quad \forall t \in [t_0, t_f'], \tag{20b}$$

This process may continue, as shown in Fig. 3 until a feasible solution is determined or the constraint $t_f' \leq T_{\max}$ is violated. Thus, we define the maximum number of iterations allowed for every candidate pair. If the maximum number of iterations is reached, we proceed with the next candidate pair index.

Remark 2. Despite time relaxation, problem (20) can still be infeasible if d_{start} is small or if the constraint (9a) is active at t_0. Therefore, CAV C can abort the maneuver and wait a specified time interval for the next opportunity window. Otherwise, a "selfish" maneuver may be performed as in Chen et al. (2022) by computing the minimum feasible terminal time and minimum terminal position for any i and $i+1$ with $i \in \bar{S}_C$.

3.5. Optimization procedure summary

We summarize the optimization process described above and portrayed in Fig. 3. Specifically, the overall optimization problem consists of the following steps:

1. Given the initial position for CAV C and vehicle U, as well as a maximum allowable time $T_{\max} \geq t_f^*$, we replace the candidate set $S_C(t_f^*)$ by a simpler *fixed* set denoted by $\bar{S}_C$. Then, using the set $\bar{S}_C$, the fast lane desired speed v_{flow} is estimated as in (4).
2. CAV C determines an optimal terminal time t_f^* and control $\{u_C^*(t)\}$, $t \in [t_0, t_f^*]$ for the maneuver to minimize a given objective function J_C subject to the vehicle dynamics (6), safety constraint (9a), and physical constraints (7). Moreover, its optimal terminal speed $v_C(t_f^*)$ must be close to (or exactly match) the desired speed given by the fast lane speed v_{flow}.
3. The solution t_f^* specifies the terminal position $x_C(t_f^*)$ for CAV C. This allows the computation of the trajectory for each possible candidate pair in $\bar{S}_C$. Once each of the optimal trajectories is determined, an optimal pair (i^*, i^*+1) of cooperating CAVs must be selected to minimize the disruption metric $D_{S_i}(t_f^*)$ in (15). Since $D_{S_i}(t_f^*)$ depends on the terminal states $x_i(t_f^*), x_{i+1}(t_f^*)$ in (15), its minimization depends on the optimal trajectories selected by CAVs $i \in \bar{S}_C$. This requires the determination of optimal controls $\{u_i^*(t)\}$, $t \in [t_0, t_f^*]$ for all $i \in \bar{S}_C$ minimizing a given objective function J_i (to be defined in the sequel) subject to the vehicle dynamics (6) and constraints (7), (9b), (9c), and (9d).
4. We determine an optimal pair (i^*, i^*+1) which minimizes the disruption metric $D_{S_i}(t_f^*)$ over all $i \in \bar{S}$. This solution must satisfy $D_{S_i}(t_f^*) \leq D_{th}$.

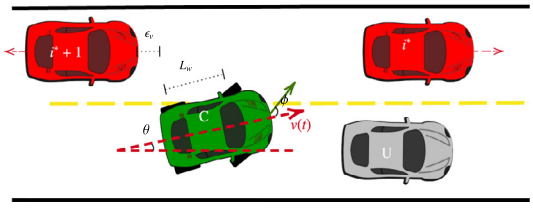

Fig. 4. Lateral dynamics diagram.

4. Lateral optimal control solution

In this paper, the lateral component of the maneuver is no different than the one presented in Chen et al. (2022) for the purely vehicle-centric lane-changing maneuver. In this section, we limit ourselves to an overview of this lateral maneuver component. Let t_0^L be the start time of the lateral phase of the lane-change maneuver. The most conservative approach is to set $t_0^L = t_f^*$, the optimal terminal time of the longitudinal phase. However, depending on the "aggressiveness" of a driver we may select $t_0^L \leq t_f^*$ as further discussed in this section.

The vehicle dynamics used during the lateral maneuver are expressed as

$$\begin{aligned} &\dot{x}(t) = v(t)cos\theta(t), \ \dot{y}(t) = v(t)sin\theta(t) \\ &\dot{\theta}(t) = v(t)tan\phi(t)/L_w, \ \dot{\phi}(t) = \omega(t) \end{aligned} \tag{21}$$

where the physical interpretation of all variables above is shown in Fig. 4. Specifically, we denote $x(t)$, $y(t)$, $v(t)$, $\theta(t)$, and $\phi(t)$ as CAV C states representing the longitudinal position, lateral position, speed, heading angle, and steering angle, respectively. Similarly, we define $\omega(t)$ and $u(t)$ as the control inputs for CAV C denoting the angular acceleration, and acceleration of the vehicle, respectively. Lastly, we denote L_w as the wheel length distance. We impose physical constraints as follows:

$$|\phi(t)| \leq \phi_{max}, \ |\theta(t)| \leq \theta_{max} \tag{22}$$

The associated initial conditions are $\phi(t_0^L) = 0$, $\theta(t_0^L) = 0$, $y(t_0^L) = 0$. The terminal time is defined as t_f^L and the associated terminal conditions are

$$\phi(t_f^L) = 0, \ \theta(t_f^L) = 0, \ y(t_f^L) = l \tag{23}$$

where l is the lane width.

4.1. Optimal control problem formulation

Once defined the vehicle's lateral dynamics together with its physical constraints, the optimal control problem for the lateral maneuver is formulated as

$$\min_{\phi(t), t_f^L} \int_{t_0^L}^{t_f^L} \frac{1}{2} w_\phi \phi^2(t) dt + w_{t_f^L} t_f^L \tag{24}$$

s.t. (21), (22), (23)

where the objective function combines both the lateral maneuver time and the associated energy of the controllable vehicle (approximated through the integral of $\phi^2(t)$) above. The two terms

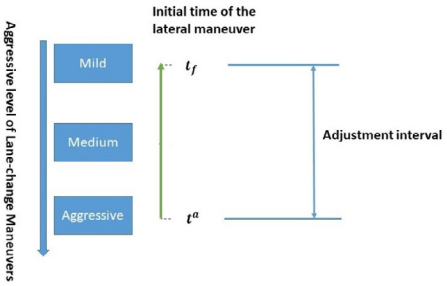

Fig. 5. Maneuver aggressiveness.

in Fig. 4 need to be properly normalized, therefore, we set $w_\phi = \frac{\rho^L}{\phi^2_{\max}}$ and $w_{t_f^L} = \frac{1-\rho^L}{T^L_{fmax}}$, where $\rho^L \in [0, 1]$ and T^L_{fmax} is set based on an empirical value. We assume that $v(t) = v$ is constant over the lateral maneuver, which is reasonable since, as shown in Chen et al. (2022), the lateral phase time is much smaller compared to the longitudinal phase. For a complete detailed solution to problem (24), we direct the reader to Chen et al. (2022).

4.2. Combination of longitudinal and lateral maneuvers

After addressing the longitudinal and lateral maneuver components separately, we next consider how to integrate them into a complete lane change maneuver. The initial time t_0^L for the lateral maneuver phase is associated with a preset driver "aggressiveness" level. As illustrated in Fig. 5, the most conservative approach is to not execute the lateral maneuver until the longitudinal phase is complete, i.e., set $t_0^L = t_f$. The most aggressive approach is determined by the earliest time at which CAV C would merge in between i^* and $i^* + 1$, that is the time t_0^L at which any adjacent vehicle along the longitudinal direction can be guaranteed to not collide with CAV C.

Once the optimal cooperative pair is chosen, let us define the earliest times when CAV C has reached a safe distance form each of the other three CAVs involved in the longitudinal maneuver in Fig. 1. Thus, we define τ_j s.t. $j \in \{i^*, i^*+1, U\}$ as the earliest times at which CAV C has reached a safe terminal position in accordance to (9b), (9c), and (9a) respectively. Thus, τ_j is defined as follows:

$$\tau_{i^*} = \min\{t \in [t_0, t_f] : x_{i^*}(t) - x_C(t) \geq \epsilon_v\} \tag{25a}$$

$$\tau_{i^*+1} = \min\{t \in [t_0, t_f] : x_C(t) - x_{i^*+1}(t) \geq \epsilon_v\} \tag{25b}$$

$$\tau_U = \min\{t \in [t_0, t_f] : x_U(t) - x_C(t) \geq \epsilon_v\} \tag{25c}$$

where ϵ_v denotes a minimum safe distance similar to (8), typically determined by the length of CAV C. We then define the lateral maneuver starting time $t_0^L = t^a$ as follows:

$$t^a = \max\{\tau_{i^*}, \tau_{i^*+1}, \tau_U\} \tag{26}$$

Remark 3. Setting the lateral maneuver starting time $t_0^L = t^a$ may not always be feasible due to the assumption of constant speeds over the lateral maneuver. However, collision avoidance can still be guaranteed similar to Section 3.4, where the longitudinal maneuver time can be extended to allow larger gaps between i^* and $i^* + 1$ and consequently longer adjustment intervals.

Remark 4. We can extend the maneuver execution to perform a series of individual maneuvers following Fig. 3 indexed by k that minimizes the aggregate metric $D_{\text{Total}} = \sum_{k=1}^{N} D^k_{S_i}(t_f^{*k})$. For each maneuver k we compute a series of system-centric (social) optimal trajectories that start sequentially by defining a CAV C as soon as the maneuver $k-1$ has completed its corresponding lateral phase. Thus, the initial time for maneuver k is upper bounded by the terminal time of maneuver $k-1$ $\left(t_0^k \geq t_f^{k-1}\right)$. Note that CAV C for maneuver $k-1$ can become a CAV candidate for the kth maneuver. It is also possible to *parallelize* several such maneuvers by allowing them to start simultaneously given a set of target vehicles (CAV C).

5. Simulation results

This section provides simulation results illustrating the time and energy-optimal controllers we have derived and comparing their performance against a baseline of non-cooperating (e.g., human-driven) vehicles. Our results are based on using the traffic simulation software package PTV Vissim where we use the included COM API to control the vehicles involved in each lane-changing maneuver. We only relinquish control for the duration of each maneuver and return it to PTV Vissim after the maneuver has ended.

Our simulation setting consists of a straight two-lane highway segment 4000 m long and an allowable speed range of $v = [10, 35]$ m/s. The incoming traffic is spawned with a desired speed of $v_{flow} = 34$ m/s. Similarly, the inter-vehicle safe distance (8) is given by $\varepsilon = 1.5$ m and headway parameter φ drawn from a normal distribution $\mathcal{N}(0.6,\ 0.4)$ s set to represent tighter bounds due to the assumption of a road composed by 100% CAVs with communication capabilities. To simulate congestion generation, we spawn an uncontrolled vehicle U traveling on the right lane (slow lane) with a constant speed $v_U = 16$ m/s throughout the simulation. The corresponding CAV C is defined as vehicle U's immediately following vehicle. For the maneuver start distance we select d_{start} from $\mathcal{N}(70, 10)$ m for every CAV C initiating a maneuver. To find the possible CAV candidates on the fast lane, we choose $L_f = 50m$ and $L_r = 80$ m in setting the candidate set $\bar{S}_C$ in (3). The control limits specified for every CAV are given by $u_{\min} = -7$ m/s^2 and $u_{\max} = 3.3$ m/s^2. The minimum safety distance to perform a lane change was defined as $\epsilon_v = 9\,m$ which includes an average vehicle length of 4 m. It is assumed that all CAVs in all simulation scenarios share the same parameters and control bounds. Lastly, we run our simulations on an AMD Ryzen 9 5900x 3.7 GHz. For simplicity, we use CasADi Andersson et al. (2019) as a numerical solver and IPOPT as an interior point optimizer for the computation of the OCP solutions. We employ a numerical solution in order to assess the worst-case time performance for the computation of the trajectories corresponding from solving problems (17a), (18), (19), and (20) respectively. The computational time can be substantially decreased by taking advantage of the analytical solutions derived in Appendix A.1.

5.1. CAV C longitudinal maneuver

We apply the formulation proposed for CAV C in (17a) for different settings using the desired fast lane speed $v_{flow} = 30$ m/s. Thus, we provide simulation results for the initial conditions pertaining only to vehicles U and C as described in Table 1 for Cases 1 and 2. For Case 1, we show a sample trajectory generated from the relaxation of the optimal time proposed in (20) with the relaxation factor $\lambda_{t_f} = 1.1$. Additionally, we define the weighting factors in (17a) as $w_v = 0.25$, $w_t = 0.55$, and $w_u = 0.2$. It can be seen for Case 1, when $d_{\text{start}} = 50$ m, the resulting maneuver time is $t_f^* = 2.7$ s, and a linear control strategy of constant acceleration to reach v_{flow} is shown in Fig. 6(a). Conversely, for Case 2, when the resulting relaxed maneuver time is $t_f^* = 3.6$ s given that CAV C needs to first undergo a deceleration segment to provide enough space to undergo a final acceleration segment allowing CAV C to get close to v_{flow} without violating the safety constraint (9a) as shown in Fig. 6(b). Finally, numerically solving the OCP

Table 1
Vehicle C sample results.

Description \ States	Relaxed	d_{start} [m]	$x_U(t_0)$ [m]	$v_U(t_0)$ [m/s]	$x_C(t_0)$ [m]	$v_C(t_0)$ [m/s]	t_f [s]	$v_C(t_f)$ [m/s]
Case 1	False	50	50	16	0	23	2.73	29.53
Case 2	True	50	50	16	0	23	3.63	29.57

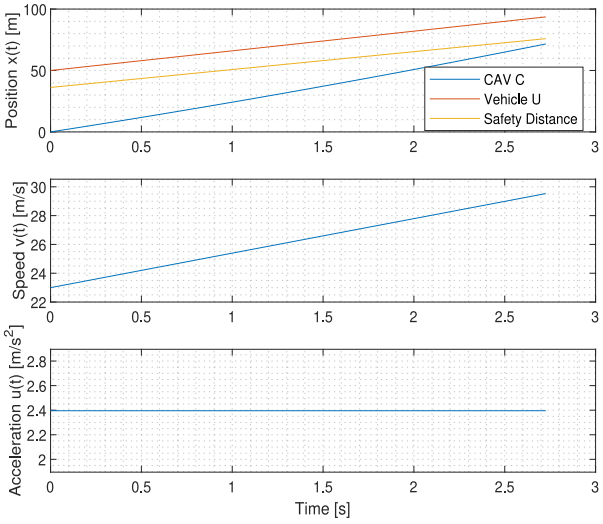

(a) Case 1: Constant acceleration with no time relaxation

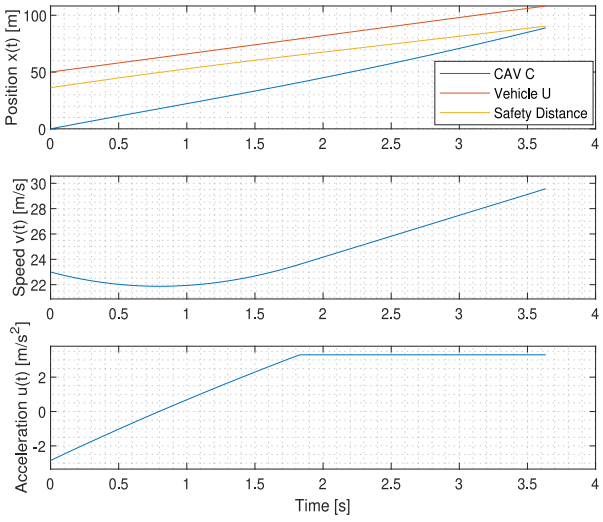

(b) Case 2:Mixed acceleration under time relaxation

Fig. 6. Sample optimal trajectory solutions for CAV C.

(17a) with a time discretization of 250 points (this is the hardest problem to solve due to the non-convexity of its objective), we obtain results that take an average of 611 ms to obtain. Similarly, we obtained an average computation time of 85 ms for OCP (20) with similar computation times for OCPs (18) and (19).

5.2. Sequential maneuvers

We also implemented a series of optimal maneuvers taking into account the system-centric goal of minimizing throughput disruptions. Unlike our previous study in Chavez Armijos et al. (2022), the disruption metric now includes a speed disruption component.

The maximum disruption value used for this study was given as $D_{\text{th}} = 0.15$, with the weight factor $\gamma = 0.8$ for position and $1-\gamma = 0.2$ for velocity in (10). In the optimal control problem (OCP) (17a) for CAV C, the weight factors are given as $w_t = 0.55$, $w_v = 0.25$ and $w_u = 0.2$ to penalize maneuver time, terminal velocity costs, and energy consumption, respectively. The disruption for CAV i^* is set as 0 since the speed of CAV i^* will never decrease, and the weights ζ_C, ζ_{i^*+1} for CAV C and CAV i^*+1 in (15) are 0.5 and 0.5, respectively. When calculating the desired speed of the fast lane v_{flow} in (5), we set $\omega = 0.3$ as the weight on the average speed and $1-\omega = 0.7$ as the weight on the maximum speed. When computing the disruption, the maximum disruption allowed was defined as $D_{th} = 0.15$. For simulation purposes, we allowed up to ten relaxations per candidate pair. The throughput analysis is performed by counting the number of vehicles within a 240 s window that crosses a measurement point at 4000 m from the starting line. To investigate the effectiveness of our controllers over different traffic rates, we performed simulations under traffic rates of 2000, 3000, 4000, and 5000 vehicles/hour, respectively. We collected data to obtain statistics for throughput, maneuver time, number of completed maneuvers, and average travel time for a CAV to pass the specific segment so as to make comparisons to the baseline case of 100% human-driven vehicles (HDVs) in Vissim.

Performance results for optimally controlled CAVs and non-cooperating vehicles under different traffic rates are summarized in Table 2. We use "OCMs" and "Baseline" to represent cooperative Optimal Control Maneuvers and non-cooperative human-driven cases, respectively. Table 2 shows that the throughput improvement of our OCMs strategies increases from 4.31% to 16.46% compared to the baseline as the traffic rates increase from 2000 to 5000. Meanwhile, the maneuver time of CAV C is around 7s in the OCMs, while it takes a vehicle without any cooperation benefit more than 30 s to complete a lane change maneuver in the baseline. The average maneuver time for CAVs decreases by about 80%, which in turn reduces vehicle energy consumption when a lane change is performed. Additionally, the number of CAVs completing the maneuver in OCMs increases by at least 225% and up to 762.5%, and the average travel time for a CAV to pass the segment is reduced by 3.53% to 9.29% when traffic rates increase from 2000 to 5000 respectively. Moreover, we provide bar charts for the throughput, maneuver time, and the number of CAV C maneuvers comparing the different performance metrics under several traffic rates as shown in Figs. 7(a), 7(b), and 7(c) respectively. These include the mean value and standard deviation under different traffic rates for both OCMs and baseline cases. The differences for each pair in these charts are statistically significant, indicating that optimally controlled CAVs experience significantly improved baseline performance, while also resulting in improved OCM throughput.

In addition, we compare the performance of OCMs with the case where vehicles still optimally control their acceleration, but there is no longer any optimal cooperative pair selection. Instead, CAV C adopts the "greedy policy" of cooperating with its immediate leader and the immediate follower on the fast lane, respectively. Thus, (16) is no longer applied. The "greedy policy" is equivalent to the approach proposed by Chen et al. (2022). This benefits the "selfish" objective of achieving shorter maneuver times at the expense of the "social" objective of improving throughput. The results are summarized in Table 3. As expected,

Table 2
Throughput analysis comparison between OCMs and human driving baseline on a 4000 m highway segment under different traffic rates.

Traffic rate [veh/hour]	Throughput [veh/hour]			Maneuver time [s]			Number of completed maneuvers (in 240 s)			Avg. travel time [s]		
	OCMs	Baseline	Difference [%]	OCMs	Baseline	Difference [%]	OCMs	Baseline	Difference [%]	OCMs	Baseline	Difference [%]
2000	1017	975	4.31	6.01	29.21	−79.42	26.00	8.00	225.00	139.01	144.10	−3.53
3000	1251	1155	8.31	6.06	44.20	−86.29	36.30	5.00	626.00	144.53	151.04	−4.31
4000	1350	1170	15.38	6.33	53.89	−88.25	34.50	4.00	762.50	148.37	158.77	−6.55
5000	1380	1170	17.95	6.54	32.50	−79.88	32.00	6.00	433.33	149.02	164.28	−9.29

Table 3
Throughput analysis comparison between OCMs and heuristic CAV selection on a 4000 m highway segment under different traffic rates.

Traffic rate [veh/hour]	Throughput [veh/hour]			Maneuver time [s]			Number of completed maneuvers (in 240 s)			Avg. travel time [s]		
	OCMs	Heuristic	Difference [%]	OCMs	Heuristic	Difference [%]	OCMs	Heuristic	Difference [%]	OCMs	Heuristic	Difference [%]
2000	1017	1015	0.20	6.01	6.21	−3.17	26.00	27.83	−6.59	139.01	140.16	−0.82
3000	1251	1176	6.41	6.06	5.64	7.47	36.30	35.88	1.18	144.53	146.94	−1.64
4000	1350	1189	13.51	6.33	5.74	10.36	34.50	39.71	−13.13	148.37	154.97	−4.26
5000	1380	1203	14.71	6.54	5.55	17.75	32.00	37.40	−14.44	149.02	157.68	−5.49

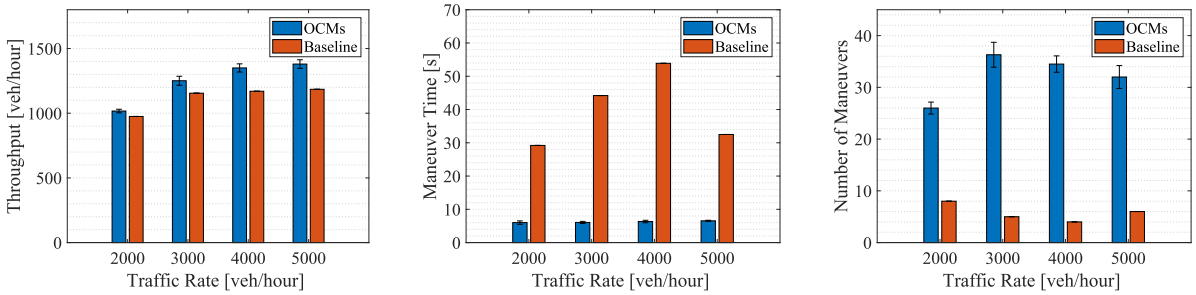

(a) Throughput (b) Maneuver Time (c) Total Completed Maneuvers

Fig. 7. Maneuver impact on network performance.

Table 4
Energy comparison between OCMs and heuristic CAV selection on a 4000 m highway segment under different traffic rates.

Traffic rate [veh/hour]	Avg. energy ($\frac{1}{2}u^2$)			Avg. fuel consumption [mL/s]		
	OCMs	Baseline	Difference [%]	OCMs	Baseline	Difference [%]
2000	726	1217	−40.3	108140	137810	−21.5
3000	2958	3278	−9.8	216330	257460	−16.0
4000	7169	7514	−4.6	400060	448130	−10.7
5000	13270	19408	−31.6	569460	777420	−26.8

the OCM approach in Table 2 achieves better throughput at the expense of slightly longer maneuver times; however, note that the overall average travel time in Table 3 is still improved relative to the heuristic.

Lastly, Table 4 presents a comparison of the average energy consumption and average fuel consumption between optimally controlled CAVs (OCMs) and non-cooperating human-driven vehicles (baseline) at different traffic rates. Fuel consumption is modeled based on equations from Kamal et al. (2013) that account for cruise and acceleration components. Additionally, it is assumed that negative acceleration does not generate fuel consumption. Overall, the table highlights the potential benefits of optimally controlling CAVs to improve fuel efficiency and reduce emissions. The improvements in energy consumption using the u^2 metric are consistent with the more detailed fuel consumption model.

5.3. Sensitivity analysis

In this section, we wish to quantify the effect that each of the several parameters used in our analysis can have on the performance of an individual maneuver, as well as their impact on the overall traffic network performance. Thus, we have performed a sensitivity analysis on the maneuver times and the number of maneuvers as the individual (vehicle-centric) performance metrics. Similarly, we analyzed the average throughput on each simulation run as a metric for traffic network (system-centric) performance. Specifically, using a similar simulation setup as in Section 5.2 with a total simulation length of 240 s, we performed three sets of experiments by modifying parameters ω defined in (4), γ defined in (10), and ζ_i defined in (15). A summary containing the parameters used for the sensitivity analysis is shown in Table 5. Similarly, the averaged results over each corresponding set of parameters are shown in Fig. 8.

It can be seen from Fig. 8 that for the position disruption weight γ, the overall number of performed maneuvers did not change much on average. However, it can be seen that whenever $\gamma \geq 0.75$ the throughput starts seeing a dramatic decrease in magnitude. On the contrary, with increasing γ, a monotonic increase in the average maneuver time can be observed, with a particular emphasis when the speed disruption contribution is almost null. This shows the overall need for the speed disruption contribution.

On a similar note, it can be seen that the weight ω used in the fast lane desired speed estimate plays a significant role in the average number of maneuvers performed. Similarly, it can be seen that the average throughput behaves proportionally with the average number of maneuvers influenced by the changes in ω. The optimal behavior can be seen to occur whenever $\omega \approx 0.25$, meaning that a larger weight should be given to $v_{\max}$. The aforementioned behavior can be explained given that the average traffic speed is only given by a smaller subset $\bar{S}_C$ of the high-speed lane which might have been disrupted by a previous maneuver, but the overall fast lane desired speed might be much higher. Nevertheless, whenever only using $v_{flow} = v_{\max}$ (or $\omega = 0$), it can be seen that the overall maneuver length is increased significantly with a proportional decrease in throughput.

Table 5
Parameters used in the different evaluation scenarios. Each row represents a distinct simulated scenario, with parameters varying one at a time across scenarios for generating the results in Fig. 8.

Traffic Density [veh/h]	Number Runs	D_{th}	ω	γ	ζ_1	ζ_2	ζ_C	$\zeta_2+\zeta_C$
3000	5	0.15	0	0.8	0	0.5	0.5	1
3000	5	0.15	0.25	0.8	0	0.5	0.5	1
3000	5	0.15	0.5	0.8	0	0.5	0.5	1
3000	5	0.15	0.75	0.8	0	0.5	0.5	1
3000	5	0.15	1	0.8	0	0.5	0.5	1
3000	5	0.15	0.3	0	0	0.5	0.5	1
3000	5	0.15	0.3	0.25	0	0.5	0.5	1
3000	5	0.15	0.3	0.5	0	0.5	0.5	1
3000	5	0.15	0.3	0.75	0	0.5	0.5	1
3000	5	0.15	0.3	1	0	0.5	0.5	1
3000	3	0.15	0.5	0.8	0.5	0.5	0	0.5
3000	3	0.15	0.5	0.8	0.4	0.2	0.4	0.6
3000	3	0.15	0.5	0.8	0.33	0.33	0.34	0.67
3000	3	0.15	0.5	0.8	0	0.5	0.5	1

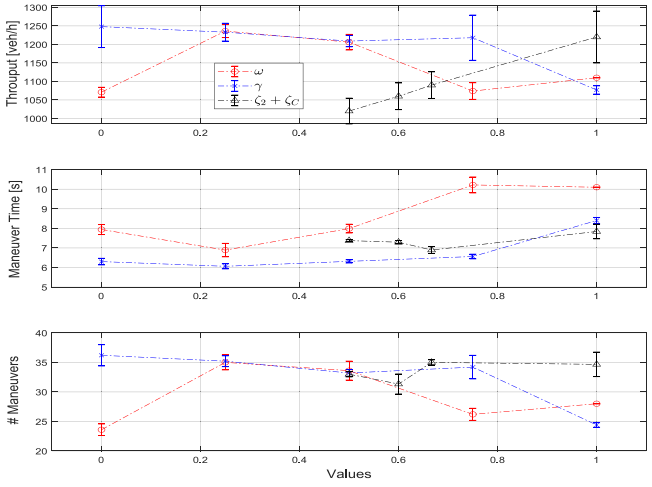

Fig. 8. Sensitivity analysis.

Lastly, the overall effect of ζ_i in (15) is analyzed by varying the split contributions of every CAV C, i^*, and i^*+1 involved in each maneuver. It can be seen that the effect on varying ζ_i does not impact the average number of maneuvers for each run. However, it can be observed from the throughput analysis that the behavior is linear with the highest throughput obtained when $\zeta_1 = 0$. Such high throughput, however, comes at the expense of slightly higher maneuver times. This phenomenon is consistent with Theorem 1 in Chen et al. (2022) where CAV i^* can only accelerate or maintain its speed, thus making its possible disruption contribution negligible.

6. Conclusions

We have developed a decentralized optimal control framework for multiple cooperating CAVs that combines the "vehicle-centric" objective of minimizing the maneuver time and energy consumed by all cooperating CAVs and the "system-centric" objective of minimizing throughput disruption in the fast lane. Our analysis includes the selection of an optimal cooperation pair of CAVs within a neighboring candidate set that minimizes a disruption metric for the fast lane traffic flow to ensure it never exceeds a given threshold. Simulation results show the effectiveness of the proposed controllers with improvements of up to 16% and 90% in average throughput and maneuver time respectively when compared to maneuvers with no vehicle cooperation. Ongoing work aims to perform multiple maneuvers simultaneously while still minimizing traffic disruption. An important next step is to extend our analysis to a mixed-traffic setting with both CAVs and human-driven vehicles (HDVs). Future work will incorporate more complex models and investigate how to bridge the gap between modeling and real-world execution.

Appendix. Analytical OCP solution

A.1. CAV C trajectory Hamiltonian analysis

The solution of the OCP (17) for CAV C can be analytically obtained by standard Hamiltonian analysis. To simplify the expression of the objective, we set the parameters $\alpha_t = w_t/w_u$, $\alpha_v = w_v/w_u$ where $w_{\{t,v,u\}}$ are the adjustable non-negative weights in (17). The Lagrange multipliers $\mu_1, \mu_2, \mu_3, \mu_4, \mu_5$ are positive when their corresponding constraints are active and become 0 when the constraints are inactive. Note that the problem has an unspecified terminal time t_f, and the terminal condition for t_f is contained in the objective. As in Bryson (2018), the terminal cost is given as $\Phi := \frac{\alpha_v}{2}[v_C(t_f) - v_{flow}]^2$ which is not an explicit function of time, and the transversality condition for (17) is

$$(\Phi_t + H)|_{t=t_f} = H(\mathbf{x_C}(t), \boldsymbol{\lambda_C}(t), u_C(t))|_{t=t_f} = 0, \tag{A.1}$$

with the costate boundary conditions

$$\lambda_C^x(t_f) = (\frac{\partial \Phi}{\partial x_C})|_{t=t_f} = 0,$$
$$\lambda_C^v(t_f) = (\frac{\partial \Phi}{\partial v_C})|_{t=t_f} = \alpha_v[v_C(t_f) - v_{flow}].$$

The Euler–Lagrange equations are given as

$$\dot{\lambda}_C^x = -\frac{\partial H}{\partial x_C} = -\mu_5,$$
$$\dot{\lambda}_C^v = -\frac{\partial H}{\partial v_C} = -\lambda_C^x + \mu_3 - \mu_4 - \varphi\mu_5, \tag{A.2}$$

and the necessary condition for optimality is

$$\frac{\partial H}{\partial u_C} = u_C(t) + \lambda_C^v(t) - \mu_1 + \mu_2 = 0. \tag{A.3}$$

A.1.1. Control, state, safety constraints inactive

In this case, the constraints in (6) are inactive for all $t \in [t_0, t_f]$, and we have $\mu_1 = \mu_2 = \mu_3 = \mu_4 = \mu_5 = 0$. Applying the Euler–Lagrange equations in (A.2), we get $\dot{\lambda}_C^x = -\mu_5 = 0$ and $\dot{\lambda}_C^v = -\lambda_C^x(t)$, which imply that $\lambda_C^x = a$ and $\lambda_C^v = -(at + b)$,

respectively. The parameters a, b here are integration constants. From (A.3), we have

$$u_C(t) + \lambda_C^v(t) = 0, \tag{A.4}$$

and $u_C(t) = -\lambda_C^v(t) = at + b$. Moreover, considering the boundary condition of the costate vector at time t_f, we have

$$\lambda_C^x(t_f) = \frac{\partial \Phi}{\partial x}|_{t=t_f} = 0, \tag{A.5}$$

which indicates that $\lambda_C^x(t) = a = 0$ for all $t \in [t_0, t_f]$, and we get $\lambda_C^v(t) = -b$ and $u_C(t) = b$ for all $t \in [t_0, t_f]$. Furthermore, we have $\alpha_v[v_{flow} - v_C(t_f)] = b$ according to the costate boundary condition.

From (A.1), the transversality condition gives the following relationship

$$\frac{1}{2}u_C^2(t_f) + \alpha_t + \lambda_C^x(t_f)v_C(t_f) + \lambda_C^v(t_f)u_C(t_f) = 0, \tag{A.6}$$

and recalling that $u_C(t) = b$, it follows that $b = \pm\sqrt{2\alpha_t}$ and $u_C(t) = \pm\sqrt{2\alpha_t}$. Consequently, we obtain the following optimal solution for $t \in [t_0, t_f]$:

$$u_C^*(t) = b = \pm\sqrt{2\alpha_t}, \tag{A.7}$$

$$v_C^*(t) = v_0 \pm \sqrt{2\alpha_t}(t - t_0), \tag{A.8}$$

$$x_C^*(t) = x_C(t_0) + v_0(t - t_0) \pm \frac{1}{2}\sqrt{2\alpha_t}(t - t_0)^2. \tag{A.9}$$

Furthermore, the costate condition and (A.8) provide the terminal time t_f as

$$t_f^* = t_0 + \frac{\alpha_v(v_{flow} - v_0) \mp \sqrt{2\alpha_t}}{\pm\alpha_v\sqrt{2\alpha_t}}. \tag{A.10}$$

Observe that in this case, the optimal control input is a time-invariant acceleration. The sign of the optimal control $u_C^*(t)$ depends on the initial speed $v_C(t_0)$.

A.1.2. Some constraints active

Define $\bar{x}_C(t_f)$ as the terminal position of CAV C if $u_C(t) = 0$ for all $t \in [t_0, t_f]$, and $x_C(t_f)$ as the actual terminal position of CAV C. Then, we can specify several cases depending on the relationship between $\bar{x}_C(t_f)$ and $x_C(t_f)$. Following the same analysis as in Chen et al. (2022), there only exist three feasible cases under which the safety constraints are satisfied:

Case 1: $\bar{x}_C(t_f) \le x_C(t_f) \le x_U(t_f) - \delta_C$

If $\bar{x}_C(t_f) \le x_C(t_f)$, then $u_C^*(t) \ge 0$ and $u_C(t) = -\sqrt{2\alpha_t}$ is infeasible. For $u_C(t) = \sqrt{2\alpha_t}$, we consider whether the velocity, acceleration, and safety constraints are active or not.

Firstly, we consider the control constraint. Since $u_C(t) = \sqrt{2\alpha_t}$ is a constant acceleration which only depends on α_t, we can easily compare it with $u_{C,\max}$ and $u_{C,\min}$. If $\sqrt{2\alpha_t} > u_{C,\max}$, then $u_C^*(t) = u_{C,\max}$; if $\sqrt{2\alpha_t} < u_{C,\max}$, then the acceleration constraint will never be activated in this case.

Secondly, we consider the velocity constraint. Since CAV C accelerates to v_{flow} with constant acceleration $u_C(t) = \sqrt{2\alpha_t}$, we only need to compare $v_C(t_f)$ to v_{flow}. Since the desired velocity v_{flow} has to satisfy $v_{flow} \le v_{C,\max}$ and we have $u_C(t) \ge 0$, it follows that the velocity constraint will never be activated in this case.

Finally, we check the safety constraint. Suppose at time $t_1 \in [t_0, t_f)$ the safety constraint is active under $u_C(t) = \sqrt{2\alpha_t}$. Then, $x_C(t_1) = x_U(t_1) - [\varphi v_C(t_1) + \varepsilon]$. At time t_1^-, the position of CAV C satisfies $x_C^*(t_1^-) < x_U(t_1^-) - [\varphi v_C(t_1^-) + \varepsilon]$, and we must have $v_C(t_1^-) > v_U$ to activate the safety constraint. With the continuity of $x_C(t)$, $v_C(t)$ and $u_C(t) \ge 0$, the position of CAV C at time t_1^+ should satisfy $x_C^*(t_1^+) > x_U(t_1^+) - [\varphi v_C(t_1^+) + \varepsilon]$. With $u_C(t) \ge 0$, we will eventually have $x_C(t) > x_U(t) - [\varphi v_C(t) + \varepsilon]$ for all $t \in (t_1, t_f]$, which contradicts the safety condition (6). Therefore, the safety constraint will never be activated for all $t \in [t_0, t_f]$ in this case.

Observe that in the analysis of Case 1, we apply $u_C(t) = \sqrt{2\alpha_t}$ to check all constraints and have not determined the value of α_t. Therefore, if $\sqrt{2\alpha_t} > u_{C,\max}$ and the acceleration constraint is activated, we apply $u_{C,\max}$ instead. Then, the difference between $v_C(t_f)$ and v_{flow} will be larger, so the speed and safety constraints will not be activated.

Case 2: $x_C(t_f) \le \bar{x}_C(t_f) \le x_U(t_f) - \delta_C$

If $x_C(t_f) \le \bar{x}_C(t_f)$, then $u_C^*(t) \le 0$ and $u_C(t) = \sqrt{2\alpha_t}$ will be infeasible in this case. With the same analysis as in Case 1, $v_C(t)$ decelerates from v_0 to v_{flow}, hence $v_C(t)$ will not reach $v_{C,\min}$ since v_{flow} satisfies $v_{flow} \ge v_{C,\min}$. Moreover, the safety constraint will not be activated for a reason similar to the one in Case 1.

Case 3: $x_C(t_f) \le x_U(t_f) - \delta_C \le \bar{x}_C(t_f)$

For $x_C(t_f) \le x_U(t_f) - \delta_C \le \bar{x}_C(t_f)$, then $u_C^*(t) = -\sqrt{2\alpha_t}$. We can check if the control constraint will be activated for all $t \in [t_0, t_f]$. Thus, we only consider the speed and safety constraints next.

Firstly, suppose only the speed constraint is active. Proceeding as in Case 1, the maximum speed constraint will not be activated. We only need to check if the minimum speed constraint is activated or not. Assume CAV C reaches $v_{\min}$ at t_1, then $t_1 = t_0 + \frac{v_{\min} - v_C(t_0)}{-\sqrt{2\alpha_t}}$. However, after CAV C enters the minimum speed-constrained arc, there is no hard terminal constraint to let C exit this arc.

Secondly, suppose only the safety constraint is activated at time $t_2 \in [t_0, t_f)$. We then have $x_C(t_2) = x_U(t_2) - [\varphi v_C(t_2) + \varepsilon]$. To activate the safety constraint, we must have $v_C(t_2^-) > v_U$ and $x_C(t_2^-) < x_U(t_2^-) - [\varphi v_C(t_2) + \varepsilon]$. To guarantee safety, $v_C(t_2^+)$ should satisfy $v_C(t_2^+) \le v_U$, otherwise, the safety constraint will be violated by the continuity of $x_C(t)$ and $v_C(t)$. Therefore, we have $v_C(t_2) = v_U$, which is equivalent to $v_0 + u_C(t_2 - t_0) = v_U$ and t_2 can be calculated as $t_2 = t_0 + \frac{v_U - v_0}{u_C}$. Since $u_C(t) = -\sqrt{2\alpha_t} < 0$ for all $t \in [t_0, t_2]$ and $u_C(t) \le 0$ for all $t \in [t_0, t_f]$, then $v_C(t) < v_U$ for all $t \in (t_2, t_f]$ if $t_2 \le t_f$, and the constraint will not be activated again in $t \in (t_2, t_f]$. If $t_2 \ge t_f$, then the safety constraint will be inactive for all $t \in [t_0, t_f]$. However, it is impossible to get $t_2 \ge t_f$, since $v_U < v_{flow}$, otherwise there is no reason for CAV C to change its lane.

Lastly, if the two constraints are active, we need to figure out the activation order. If the minimum speed constraint is activated first with $v_{\min} < v_U$, the safety constraint will not be activated for all $t \in (t_1, t_f]$. Since the safety constraint is only activated instantaneously at $t_2 \le t_f$, the two constraints being active is equivalent to only the minimum speed constraint being active.

From the analysis above, we have proved that the safety constraint may only be activated instantaneously at $t_2 \le t_f$ for $v_U < v_{flow}$, which can be omitted, and then enter the minimum speed constrained arc. For $t \in (t_1, t_f]$, there are two possible trajectories for CAV C. One is to maintain $v_{\min}$, then $t_f = t_1$ for optimality (otherwise, the time component in (A.11b) increases while the other two remain fixed). Another trajectory is to accelerate again at $t_3 < t_f$. If the safety constraint is inactive for all $t \in (t_3, t_f]$, i.e., $x_U(t) - x_C(t) > \delta_C(v_C(t)), \forall t \in (t_3, t_f]$, then the problem becomes unconstrained again, which is the same as Case 1. However, this trajectory will not be optimal because it contains unnecessary deceleration during $[t_0, t_1]$ without the safety constraint being activated for all $t \in [t_0, t_f]$ and causes increased energy consumption. Therefore, the optimal trajectory for CAV C is to have the safety constraint activated at some $t_4 \le t_f$. If $t_4 < t_f$, then we have $v_C(t) = v_U$ for all $t \in [t_4, t_f]$, otherwise the safety constraint will be violated or the trajectory will be again suboptimal. The total cost is increasing for t from t_4

to t_f since it causes additional time and energy without increasing speed. To achieve optimality, we conclude that $t_4 = t_f$.

Therefore, the inequality constraint $x_U(t) - x_C(t) = \delta_C(v_C(t))$ for all $t \in [t_0, t_f]$ is equivalent to $x_U(t_f) - x_C(t_f) = \delta_C(v_C(t_f))$ and the OCP for CAV C can be rewritten as

$$\min_{t_f, u_C(t)} \frac{\alpha_v}{2}(v_C(t_f) - v_{flow})^2 + \int_{t_0}^{t_f} \left(\alpha_t + \frac{1}{2}u_C^2(t)\right) dt \tag{A.11a}$$

$$\text{s.t.} \quad \dot{x}_C(t) = v_C(t), \ \dot{v}_C(t) = u_C(t), \tag{A.11b}$$

$$u_{C_{\min}} \le u_C(t) \le u_{C_{\max}}, \quad \forall t \in [t_0, t_f] \tag{A.11c}$$

$$v_{C_{\min}} \le v_C(t) \le v_{C_{\max}}, \quad \forall t \in [t_0, t_f], \tag{A.11d}$$

$$x_U(t_f) - x_C(t_f) = \delta_C(v_C(t_f)), 0 \le t_f \le T_{\max} \tag{A.11e}$$

where the difference between (17) and (A.11) is that the safety constraint for CAV C with respect to vehicle U becomes a strict equality constraint at the terminal time t_f. The reason is that we have proved that the safety constraint may be activated instantaneously at t_2 and will never be activated again after t_2 so that the safety constraint for all $t \in [t_0, t_f)$ becomes redundant. Moreover, equality holds to save any unnecessary deceleration of CAV C. For this revised OCP, its Hamiltonian becomes

$$\begin{aligned} H(\mathbf{x_C}, \boldsymbol{\lambda_C}, u_C) &= \frac{1}{2}u_C^2(t) + \alpha_t + \lambda_C^x(t)v_C(t) + \\ &\lambda_C^v(t)u_C(t) + \mu_1(u_{C,\min} - u_C(t)) + \mu_2(u_C(t) - u_{C,\max}) \\ &+\mu_3(v_{C,\min} - v_C(t)) + \mu_4(v_C(t) - v_{C,\max}), \end{aligned} \tag{A.12}$$

the costate boundary conditions become

$$\begin{aligned} \lambda_C^x(t_f) &= (\frac{\partial \Phi}{\partial x_C})|_{t=t_f} = a, \\ \lambda_C^v(t_f) &= (\frac{\partial \Phi}{\partial v_C})|_{t=t_f} = \alpha_v[v_C(t_f) - v_{flow}], \end{aligned}$$

a is a constant, and the Euler–Lagrange equations are given as

$$\begin{aligned} \dot{\lambda}_C^x &= -\frac{\partial H}{\partial x_C} = 0, \\ \dot{\lambda}_C^v &= -\frac{\partial H}{\partial v_C} = -\lambda_C^x + \mu_3 - \mu_4. \end{aligned} \tag{A.13}$$

(1) No Constraint Active. If no constraint is active for all $t \in [t_0, t_f]$, then all Lagrange multipliers $\mu_1, \mu_2, \mu_3, \mu_4$ are 0. Thus, (A.13) gives $\dot{\lambda}_C^x = 0$, $\dot{\lambda}_C^v = -\lambda_C^x$, i.e., $\lambda_C^x = a$, $\lambda_C^v = -(at+b)$, where a, b are integration constants. With the same necessary condition for optimality in (A.3), we have

$$u_C(t) + \lambda_C^v(t) = 0, \tag{A.14}$$

which implies $u_C(t) = -\lambda_C^v(t) = at + b$. Hence, the speed and position trajectories of CAV C will be expressed as $v_C(t) = \frac{1}{2}at^2 + bt + c$ and $x_C(t) = \frac{1}{6}at^3 + \frac{1}{2}bt^2 + ct + d$, where a, b, c, d are integration constants. In addition, the transversality condition (A.1) gives the following relationship:

$$\frac{1}{2}u_C^2(t_f) + \alpha_t + \lambda_C^x(t_f)v_C(t_f) + \lambda_C^v(t_f)u_C(t_f) = 0. \tag{A.15}$$

Combining all the boundary conditions above and the initial conditions of $t_0, v_C^0, v_U, v_{flow}, \alpha_t, \alpha_v, x_C(t_0), x_U(t_0)$, the following six equations hold:

$$\begin{aligned} at_f + b &= \alpha_v(v_{flow} - v_C(t_f)), \\ v_C(t_f) &= \frac{1}{2}at_f^2 + bt_f + c, \\ v_C(t_0) &= \frac{1}{2}at_0^2 + bt_0 + c, \end{aligned}$$

$$\alpha_t + av_C(t_f) = \frac{1}{2}(at_f + b)^2, \tag{A.16}$$

$$\begin{aligned} x_C(t_0) &= \frac{1}{6}at_0^3 + \frac{1}{2}bt_0^2 + ct_0 + d, \\ x_U(t_f) - \delta_C(v_C(t_f)) &= \frac{1}{6}at_f^3 + \frac{1}{2}bt_f^2 + ct_f + d. \end{aligned} \tag{A.17}$$

Thus, the unknown variables a, b, c, d, t_f can be obtained by solving (A.17). It is also easy to show that a has to be non-negative, and b has to be non-positive. If both a, b are positive, then CAV C will never decelerate, which violates the terminal conditions for $x_C(t_f) \le \bar{x}_C(t_f)$. If both a, b are negative, then CAV C will keep decelerating, which violates the optimality in the unconstrained case. If a is negative, b is positive, this means that CAV C will accelerate over $[t_0, t_1]$ where $t_1 = -\frac{b}{a}$, then decelerate. If $t_1 \ge t_f$, which means CAV C keeps accelerating for all $t \in [t_0, t_f]$, then the terminal constraint $x_C(t_f) \le \bar{x}_C(t_f)$ will be violated. If $t_1 \le t_f$, which means CAV C accelerates in $[t_0, t_1]$, then decelerates in $[t_1, t_f]$, which violates the optimality in the unconstrained case.

(2) Safety Constraint Active Only. In this case, we can show that the safety constraint will be activated at most once instantaneously during $[t_0, t_f)$. First, note that with the initial condition $v_C(t_0) < v_{flow}$ and the terminal position $x_C(t_f) \le x_U(t_f) - \delta_C \le \bar{x}_C(t_f)$, CAV C cannot keep accelerating over $[t_0, t_f]$, otherwise we will get Case 1. If the safety constraint is activated at t_1, then $v_C(t_1) = v_U$; otherwise, if $v_C(t_1) > v_U$, then from the continuity of velocity, the safety constraint will be violated at t_1^+, whereas if $v_C(t_1) < v_U$, then the safety constraint will not be activated at t_1. Considering the value of t_1, if $t_1 \ge t_f$, then it follows that indeed the safety constraint will be activated at most once. On the other hand, if $t_1 < t_f$, there are two possible trajectories for CAV C in $t \in [t_1, t_f]$. One is to travel at constant speed such that the safety constraint is activated for all $t \in [t_1, t_f]$ with $v_C(t) = v_U$. However, to achieve optimality, t_1 should be exactly equal to t_f because the objective function in (A.11b) is monotonically increasing over $[t_1, t_f]$ with the same terminal speed cost. Another trajectory is to exit the safety-constrained arc at $t_2 < t_f$. However, to guarantee safety, C still has to decelerate at t_2, then accelerate at some t_3 such that $t_2 < t_3 < t_f$ to satisfy the terminal position constraint $x_U(t_f) - x_C(t_f) = \delta_C(v_C(t_f))$. However, decreasing the length of the safety-constrained arc will decrease the objective, hence the optimal solution is to have $t_1 = t_2$.

Therefore, having shown that the safety constraint will be activated at most once instantaneously during $[t_0, t_f)$, we now only need to consider whether the speed and control constraints are active as discussed in the remaining cases below.

(3) Control Constraint Active Only. The analysis in *(1)* indicates that the acceleration is non-decreasing, so the minimum control constraint will not be activated if it is inactive at the initial time. Firstly, we assume only the maximum control constraint is activated. Suppose $u(t)$ reaches $u_{\max}$ at time t_1. Then $u_C(t) = at + b$ for $t \in [t_0, t_1]$, $u_C(t) = u_{\max}$ for $t \in [t_1, t_f]$ and t_1 can be computed by $at_1 + b = u_{\max}$ with the obtained coefficients a, b from (A.17). Moreover, $x_C(t_1)$, $v_C(t_1)$ can also be obtained and we can express the terminal speed as

$$v_C(t_f) = v_C(t_1) + u_{\max}(t_f - t_1), \tag{A.18}$$

and the terminal position

$$\begin{aligned} &v_U(t_f - t_0) - \delta(v_C(t_f)) \\ &\qquad = x_C(t_1) + v_C(t_1)(t_f - t_1) + \frac{1}{2}u_{\max}(t_f - t_1)^2 \end{aligned} \tag{A.19}$$

to solve for the terminal time t_f.

If only the minimum control constraint is activated, since the acceleration is non-decreasing, the entry point of the constrained arc is t_0, and suppose t_2 is the exit point of the constrained arc. Similarly, we have the following six equations:

$$\begin{aligned}
&at_2 + b = u_{\min},\\
&at_f + b = \alpha_v[v_{flow} - v_C(t_f)],\\
&\frac{1}{2}at_2^2 + bt_2 + c = v_{\min},\\
&\frac{1}{6}at_2^3 + \frac{1}{2}bt_2^2 + ct_2 + d =\\
&\qquad x_C(t_0) + v_C(t_0)(t_2 - t_0) + \frac{1}{2}u_{\min}(t_2 - t_0)^2,\\
&\frac{1}{6}at_f^3 + \frac{1}{2}bt_f^2 + ct_f + d = x_U(t_f) - \delta(v_C(t_f)),\\
&\frac{1}{2}(at_f + b)^2 + \alpha_t + av_C(t_f) - (at_f + b)^2 = 0,
\end{aligned} \tag{A.20}$$

to solve for a, b, c, d, t_2, t_f.

Finally, if the minimum and maximum constraints are both activated, suppose the exit point for the minimum constraint is τ_1, and the starting point for the maximum constraint is μ_2. Then $u(t) = u_{\min}, t \in [t_0, \tau_1)$, $u(t) = at + b, t \in [\tau_1, \tau_2]$ and $u(t) = u_{\max}, t \in (\tau_2, t_f]$. Therefore, τ_1 is the same as t_2 in the above case, and we now calculate τ_2 and t_f by using $a\tau_2 + b = u_{\max}$ with

$$\begin{aligned}
&x_C(\tau_2) + v_C(\tau_2)(t_f - \tau_2)\\
&\qquad + \frac{1}{2}u_{\max}(t_f - \tau_2)^2 = x_U(t_f) - \delta(v_C(t_f))
\end{aligned} \tag{A.21}$$

$$\begin{aligned}
v_C(\tau_2) &= \frac{1}{2}a\tau_2^2 + b\tau_2 + c,\\
x_C(\tau_2) &= \frac{1}{6}at_2^3 + \frac{1}{2}bt_2^2 + ct_2 + d
\end{aligned}$$

so that we can solve for τ_2, t_f, where a, b, c, d are obtained from the Eqs. (A.20).

(4) Speed Constraint Active Only. From the terminal position, we know that CAV C includes both a deceleration and acceleration trajectory segment. Since the safety constraint will never be activated in $[t_0, t_f)$ and we have $v_{flow} < v_{\max}$, the maneuver will be completed before the maximum constraint is activated. Hence, we only need to check whether the minimum speed $v_{\min}$ is reached. Suppose t_1 is the starting point of such a constrained arc and t_2 is the exit point. Then, $u(t) = at + b$ for $t \in [t_0, t_1)$, and $u(t) = 0$ for $t \in [t_1, t_2]$. We can compute t_1 through $at_1 + b = 0$ and further express the velocity and position of CAV C at t_1 as

$$\begin{aligned}
v_C(t_1) &= \frac{1}{2}at_1^2 + bt_1 + c,\\
x_C(t_1) &= \frac{1}{6}at_1^3 + \frac{1}{2}bt_1^2 + ct_1 + d,
\end{aligned} \tag{A.22}$$

where the coefficients a, b, c, d are obtained by (A.17). Hence, we can solve the following six equations

$$\begin{aligned}
&a_1t_2 + b_1 = 0,\\
&\frac{1}{2}a_1t_2^2 + b_1t_2 + c_1 = v_{\min},\\
&a_1t_f + b_1 = \alpha_v(v_{flow} - v_C(t_f)),\\
&\frac{1}{6}a_1t_2^3 + \frac{1}{2}b_1t_2^2 + c_1t_2 + d_1 = x_C(t_1) + v_{\min}(t_2 - t_1),\\
&\frac{1}{6}a_1t_f^3 + \frac{1}{2}b_1t_f^2 + c_1t_f + d_1 = x_U(t_f) - \delta(v_C(t_f)),\\
&\frac{1}{2}(a_1t_f + b_1)^2 + \alpha_t + a_1v_C(t_f) - (a_1t_f + b_1)^2 = 0
\end{aligned} \tag{A.23}$$

to obtain $a_1, b_1, c_1, d_1, t_2, t_f$.

(5) Control and Speed Constraints Active. Based on the speed constraint analysis above, the maximum speed will not be reached during $[t_0, t_f]$. Therefore, there are only three cases that could occur if we have control and speed constraints active, i.e., (i) $u_{\min}$, $v_{\min}$ active, (ii) $u_{\max}$, $v_{\min}$ active, (iii) $u_{\min}$, $v_{\min}$ and $u_{\max}$ active.

(i) $u_{\min}$, $v_{\min}$ active: First, we need to check which constraint will be activated first. If $v_{\min}$ is reached, this indicates that the acceleration decreases to 0, and the acceleration has to be positive to exit the $v_{\min}$ constrained arc. Hence, $u_{\min}$ is reached first at $t_1 > t_0$, then reaches $v_{\min}$ at $t_2 > t_1$. Notice that for $t \in [t_0, t_1)$, the control constraint has the same performance as in *(3)*, so we use (A.20) to get the CAV C trajectory for $t \in [t_0, t_1]$ directly.

At time t_2, we have the interior constraint $N(v_C(t)) = v_{\min} - v_C(t_2) = 0$, and

$$\begin{aligned}
\lambda_C^T(t_2^-) &= \lambda_C^T(t_2^+) + \pi\frac{\partial N}{\partial \mathbf{x}}|_{t=t_2},\\
H(t_2^-) &= H(t_2^+) - \pi\frac{\partial N}{\partial t}|_{t=t_2},
\end{aligned} \tag{A.24}$$

where π is a Lagrangian multiplier. Based on (A.24), we have $\lambda_C^x(t_2^-) = \lambda_C^x(t_2^+)$, $\lambda_C^v(t_2^-) = \lambda_C^v(t_2^+) - \pi$, and $H(t_2^-) = H(t_2^+)$. Hence, we have

$$\begin{aligned}
&\frac{1}{2}u_C^2(t_2^-) + \alpha_t + \lambda_C^x(t_2^-)v_C(t_2^-) + \lambda_C^v(t_2^-)u_C(t_2^-)\\
&= \frac{1}{2}u_C^2(t_2^+) + \alpha_t + \lambda_C^x(t_2^+)v_C(t_2^+) + \lambda_C^v(t_2^+)u_C(t_2^+).
\end{aligned} \tag{A.25}$$

Since the state variables are continuous, we have $v_C(t_2^-) = v_C(t_2^+)$, $x_C(t_2^-) = x_C(t_2^+)$ and $u_C(t_2^+) = 0$. Moreover, the optimality condition gives $u_C(t_2^-) = -\lambda_C^v(t_2^-)$. Thus, we can calculate $u_C(t_2^-) = 0$ according to (A.25), i.e., $u_C(t_2) = 0$. Letting the exit point be t_3, combining the optimality and transversality conditions, we have the following six equations

$$\begin{aligned}
&\frac{1}{2}a_1t_3^2 + b_1t_3 + c_1 = v_{\min},\\
&\frac{1}{6}a_1t_3^3 + \frac{1}{2}b_1t_3^2 + c_1t_3 + d_1 = x_C(t_2) + v_{\min}(t_3 - t_2),\\
&a_1t_3 + b_1 = 0,\\
&\frac{1}{6}a_1t_f^3 + \frac{1}{2}b_1t_f^2 + c_1t_f + d_1 = x_U(t_f) - \delta(v_C(t_f)),\\
&a_1t_f + b_1 = \gamma(v_d - v_C(t_f)),\\
&\frac{1}{2}(a_1t_f + b_1)^2 + \beta + a_1v_C(t_f) - (a_1t_f + b_1)^2 = 0
\end{aligned} \tag{A.26}$$

to solve for $a_1, b_1, c_1, d_1, t_3, t_f$. Note that using the coefficients a, b, c, d in (A.20) and the known t_1, we can similarly calculate t_2 from $at_2 + b = 0$, and $v_C(t_2), x_C(t_2)$.

(ii) $u_{\max}$, $v_{\min}$ *active:* In this case, the optimality of the solution determines that $v_{\min}$ has to be reached before $u_{\max}$, otherwise, $v_{\min}$ will not be reached or the solution will not be optimal. For the minimum speed constraint being activated first, suppose t_1 is the entry point of the minimum velocity-constrained arc, t_2 is the corresponding exit point, and t_3 is the entry point of the acceleration constraint. For $t \in [t_0, t_1)$, the trajectories of CAV C have the same performance as in *(4)*, i.e., $u_C(t) = at + b, t \in [t_0, t_1)$, $u_C(t) = 0, t \in [t_1, t_2)$, and $u_C(t) = a_1t + b_1, t \in [t_2, t_3)$, where t_1, t_2, a, b, a_1, b_1 can be calculated from (A.22) and (A.23).

In addition, t_3 can be computed from $a_1 t_3 + b_1 = u_{\max}$, and we can further obtain $v_C(t_3), x_C(t_3)$.

For the terminal position constraint, the states at the terminal time t_f should satisfy the following equation:

$$x_C(t_3) + v_C(t_3)(t_f - t_3) + \frac{1}{2}u_{\max}(t_f - t_3)^2 = x_U(t_0) + v_U(t_f - t_0) - \phi v_C(t_f) - \delta,$$

which provides the solution for t_f.

(iii) $u_{\min}$, $v_{\min}$ and $u_{\max}$ active: regarding the activation order of the three constraints, $u_{\min}$, $v_{\min}$, and $u_{\max}$, proceeding as in the previous cases, $u_{\min}$ will be activated first to reach $v_{\min}$, then CAV C accelerates from $v_{\min}$ to v_{flow}, and then $u_{\max}$ is activated. We can directly combine the results of cases (i) and (ii) to get the complete trajectory for CAV C in this case.

A similar analysis can be performed for the solutions for CAVs i and $i+1$, thus we omit the details for the Hamiltonian analysis corresponding to (18), (19), and (20).

References

Andersson, J. A. E., Gillis, J., Horn, G., Rawlings, J. B., & Diehl, M. (2019). CasADi – A software framework for nonlinear optimization and optimal control. *Mathematical Programming Computation*, *11*(1), 1–36. http://dx.doi.org/10.1007/s12532-018-0139-4.

Bax, C., Leroy, P., & Hagenzieker, M. P. (2014). Road safety knowledge and policy: A historical institutional analysis of the Netherlands. *Transportation Research Part F: Traffic Psychology and Behaviour*, *25*, 127–136.

Bryson, A. E. (2018). *Applied optimal control: optimization, estimation and control*. Routledge.

Chavez Armijos, A. S., Chen, R., Cassandras, C. G., Al-Nadawi, Y. K., Mahjoub, H. N., & Araki, H. (2022). Sequential cooperative energy and time-optimal lane change maneuvers for highway traffic. In *2022 IEEE 25th international conference on intelligent transportation systems* (pp. 1623–1628). IEEE Press, http://dx.doi.org/10.1109/ITSC55140.2022.9922000.

Chen, R., Cassandras, C. G., Tahmasbi-Sarvestani, A., Saigusa, S., Mahjoub, H. N., & Al-Nadawi, Y. K. (2022). Cooperative time and energy-optimal lane change maneuvers for connected automated vehicles. *IEEE Transactions on Intelligent Transportation Systems*, *23*(4), 3445–3460. http://dx.doi.org/10.1109/TITS.2020.3036420.

He, S., Zeng, J., Zhang, B., & Sreenath, K. (2021). Rule-based safety-critical control design using control barrier functions with application to autonomous lane change. In *2021 American control conference* (pp. 178–185). IEEE.

Kamal, M. A. S., Mukai, M., Murata, J., & Kawabe, T. (2013). Model predictive control of vehicles on urban roads for improved fuel economy. *IEEE Transactions on Control Systems Technology*, *21*(3), 831–841.

Li, T., Wu, J., Chan, C.-Y., Liu, M., Zhu, C., Lu, W., & Hu, K. (2020). A cooperative lane change model for connected and automated vehicles. *IEEE Access*, *8*, 54940–54951. http://dx.doi.org/10.1109/ACCESS.2020.2981169.

Li, B., Zhang, Y., Feng, Y., Zhang, Y., Ge, Y., & Shao, Z. (2018). Balancing computation speed and quality: A decentralized motion planning method for cooperative lane changes of connected and automated vehicles. *IEEE Transactions on Intelligent Vehicles*, *3*(3), 340–350.

Luo, Y., Xiang, Y., Cao, K., & Li, K. (2016). A dynamic automated lane change maneuver based on vehicle-to-vehicle communication. *Transportation Research Part C (Emerging Technologies)*, *62*, 87–102.

Mahjoub, H. N., Tahmasbi-Sarvestani, A., Kazemi, H., & Fallah, Y. P. (2017). A learning-based framework for two-dimensional vehicle maneuver prediction over V2V networks. In *Proc. of 15th IEEE intl. conf. on dependable, autonomic and secure computing* (pp. 156–163). IEEE.

Nilsson, J., Brännström, M., Coelingh, E., & Fredriksson, J. (2015). Longitudinal and lateral control for automated lane change maneuvers. In *Proc. of 2015 American control conf.* (pp. 1399–1404).

Nilsson, J., Brännström, M., Coelingh, E., & Fredriksson, J. (2017). Lane change maneuvers for automated vehicles. *IEEE Transactions on Intelligent Transportation Systems*, *18*(5), 1087–1096.

Vogel, K. (2003). A comparison of headway and time to collision as safety indicators. *Accident Analysis and Prevention*, *35*(3), 427–433.

Wang, M., Daamen, W., Hoogendoorn, S. P., & van Arem, B. (2016). Cooperative car-following control: Distributed algorithm and impact on moving jam features. *IEEE Transactions on Intelligent Transportation Systems*, *17*(5), 1459–1471.

Wang, M., Hoogendoorn, S. P., Daamen, W., van Arem, B., & Happee, R. (2015). Game theoretic approach for predictive lane-changing and car-following control. *Transportation Research Part C (Emerging Technologies)*, *58*, 73–92.

Zhao, D., Huang, X., Peng, H., Lam, H., & LeBlanc, D. J. (2018). Accelerated evaluation of automated vehicles in car-following maneuvers. *IEEE Transactions on Intelligent Transportation Systems*, *19*(3), 733–744.

Andres S. Chavez Armijos is a Ph.D. candidate in Systems Engineering at Boston University, Boston, MA, USA. He previously obtained an M.Sc. in Systems Engineering in 2023 from Boston University and an M.Sc. in Aerospace Engineering in 2018 from Embry-Riddle Aeronautical University, Daytona Beach, FL, USA. In 2015 he obtained a B.Sc. in Aerospace Engineering from Embry-Riddle Aeronautical University. He has been recognized through awards and scholarships including the Dean's Fellowship at Boston University and the Outstanding Engineering Graduate Student of the Year at Embry-Riddle Aeronautical University. He is a member of Tau Beta Pi and Sigma Gamma Tau. His research interests include artificial intelligence, autonomous vehicles, multi-agent systems, and safe human–robot interaction.

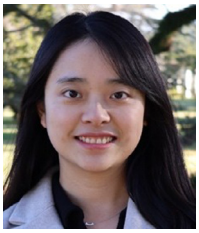

Anni Li received a B.Sc. degree in Mathematics and a minor in Physics from Central China Normal University, Wuhan, China, and an M.Sc. degree in operational research and cybernetics from Tongji University, Shanghai, China, in 2017 and 2020, respectively. She is currently working toward a Ph.D. degree in Systems Engineering at Boston University, Brookline, MA, USA. Her research focuses on autonomous vehicles in transportation systems, with emphasis on safe and optimal cooperation and methods for cooperative compliance for social optimality.

Christos G. Cassandras received a BS degree from Yale University, a M.S.E.E. degree from Stanford University, and S.B. and Ph.D. degrees from Harvard University. In 1982–1984, he was with ITP Boston, Inc. In 1984–1996, he was a Faculty Member with the Department of Electrical and Computer Engineering, University of Massachusetts/Amherst. He is currently a Distinguished Professor of Engineering at Boston University, Brookline, MA, USA, the Head of the Division of Systems Engineering, and a Professor of Electrical and Computer Engineering. He has authored or co-authored 7 books, and over 500 refereed papers in the areas of discrete event and hybrid systems, cooperative control, stochastic optimization, and computer simulation, with applications to computer and sensor networks, manufacturing systems, and transportation systems.

Dr. Cassandras serves on several journal Editorial Boards and was the Editor-in-Chief of the IEEE Transactions on Automatic Control (1998–2009). He was the 2012 President of the IEEE Control Systems Society (CSS). He has been a plenary/keynote speaker at numerous international conferences and has also been an IEEE Distinguished Lecturer. He is the recipient of several awards, including the 2011 IEEE Control Systems Technology Award, the Distinguished Member Award of the IEEE Control Systems Society (2006), the 1999 Harold Chestnut Prize (IFAC Best Control Engineering Textbook) among others. He is a Member of Phi Beta Kappa and Tau Beta Pi. He is a Fellow of the IEEE and a Fellow of the IFAC.

Yasir K. Al-Nadawi earned his Ph.D. in Electrical Engineering with a focus on control systems from Michigan State University, East Lansing, MI, USA, in 2021. He completed his M.Sc. in Control and Systems Engineering in 2008 and his B.Sc. in 2005, both from the University of Technology, Baghdad, Iraq. Since 2022, he has been serving as a Principal Research Scientist at RTX Technologies Research Center (RTRC), East Hartford, Connecticut. His current research at RTRC is dedicated to the development of safety and stability certifiable AI models and control algorithms.

This includes his work on energy management algorithms for aircraft hybrid-electric propulsion systems, which integrates reinforcement learning with deep learning-based control barrier functions. Prior to his current role, Dr. Al-Nadawi was a Research Scientist at Honda Research Institute (US) in Ann Arbor, MI. Dr. Al-Nadawi's extensive research interests transcend his institutional affiliations, encompassing the development of control systems that synergize nonlinear control systems design and analysis with certifiable machine and deep learning techniques. Throughout his career, including his previous role as a Research Scientist at Honda Research Institute (US) in Ann Arbor, MI, his work has been characterized by innovations in optimal cooperative control systems, multi-time-scale approaches, singular perturbation theory, sliding mode control theory, disturbance observers, regulation theory, reinforcement learning, physics-informed neural networks, and deep learning-based control barrier functions. Dr. Al-Nadawi's application interests span a wide range of fields, including aircraft propulsion control systems, spacesuit control systems, ground vehicle dynamics and control, autonomous driving, cooperative control, electrified powertrain control applications, and energy efficiency.

Hidekazu Araki is a chief engineer at Honda Motor Co., Ltd., Tochigi, Japan. He received his B.Eng. degree in electronics from University of Electro-Communications, Tokyo, Japan in 1996, then M.Eng. degree in engineering system from University of Tsukuba, Ibaraki, Japan in 1999. He had more than seven years of work experience in the ITS industry in Japan before starting his career in Honda. His role at Honda is focused on establishing development process and E&E platform that enable efficient mass production development. Additionally, he has provided support to research scientists at Honda Research Institute USA, Inc. specifically contributing to projects related to vehicle-to-vehicle cooperation.

Behdad Chalaki is a research scientist at Honda Research Institute USA, Inc. He earned his B.S. degree in mechanical engineering from the University of Tehran, Iran, in 2017. He furthered his education, obtaining M.S. and Ph.D. degrees from the Department of Mechanical Engineering at the University of Delaware, Newark, in 2021 and 2022, respectively. His Ph.D. research concentrated on developing online decentralized control algorithms for coordinating connected and automated vehicles (CAVs) in diverse traffic scenarios, addressing uncertainties in motion planning. His current research focuses on decision-making, motion planning, and control of multi-robot systems coexisting with humans, utilizing techniques from artificial intelligence and optimal control.

Ehsan Moradi-Pari, Ph.D. is a chief scientist and division director of Honda Research Institute USA, Inc. in Ann Arbor, Michigan. His research centers on cooperative AI and human-AI teamwork. Dr. Moradi-Pari serves as Honda's lead and representative for pre-competitive active safety research conducted at Crash Avoidance Metrics Partnership (CAMP) and the 5G Automotive Association (5GAA). He has spearheaded Honda's efforts and preparations to accelerate connected and automated vehicle deployment in the United States, including the design and deployment of the first-of-its-kind smart intersection concept in Marysville, Ohio and 5G V2X safety and mobility applications for connected and automated vehicles at the University of Michigan Mcity. In addition to his role at Honda, Dr. Moradi-Pari serves on the University of Michigan Center for Connected and Automated Transportation (CCAT) Technology Advisory Board.

His work in the area of designing communication protocols and applications for multi-agent systems including connected and automated vehicles as well as modeling and analysis of intelligent systems has been published in several international journals, conference proceedings, and book chapters.

Dr. Moradi-Pari received his doctorate degree from West Virginia University and Master of Science from Sharif University of Technology.

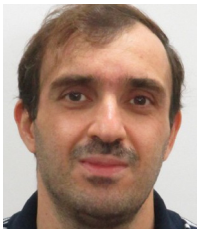

Hossein Nourkhiz Mahjoub is a research scientist at Honda Research Institute (HRI), Ann Arbor, MI, United States. He received his B.Sc. and M.Sc. degrees from University of Tehran, Tehran, Iran, in 2003 and 2008, respectively and his Ph.D. from University of Central Florida, Orlando, FL, USA in 2019, all in electrical engineering (specialized in Telecommunications Systems). He had more than nine years of work experience in the telecommunications industry before starting his Ph.D. in 2015. His research at HRI is focused on different areas, including multi-agent robotics systems, representation learning, V2X communications technologies, and stochastic systems analysis.

Vaishnav Tadiparthi is a research scientist at Honda Research Institute (HRI) in Ann Arbor, MI, USA. He earned his Bachelor's and Master's degrees in Aerospace Engineering from the Indian Institute of Technology, Kharagpur, India in 2017, and followed it up with a Ph.D. from Texas A&M University in 2022. His Ph.D. was focused on the field of scientific machine learning to understand propagation and control of uncertainty in nonlinear dynamical systems. His current research spans the domains of robotics and artificial intelligence for improving interactive decision-making in multi-agent systems using classical and learning-based methods.